University of Glasgow | Experimental Particle Physics

GLAS-PPE/2008-14
21st October 2008

Department of Physics and Astronomy
Experimental Particle Physics Group
Kelvin Building, University of Glasgow,
Glasgow, G12 8QQ, Scotland
Telephone: +44 (0)141 330 2000 Fax: +44 (0)141 330 5881

Strategies for measuring γ from the decay channels $B_d^0 \to D^{\mp}\pi^{\pm}$ and $B_s^0 \to D_s^{\mp}K^{\pm}$ at LHCb

Vladimir Vava Gligorov[1]
Guy Wilkinson[2]

[1] University of Glasgow
[2] University of Oxford

Abstract

Two possible measurements of the CKM angle γ at LHCb are evaluated: from the decay mode $B_d^0 \to D^-\pi^+$, and from the combined analysis of the decay modes $B_d^0 \to D^-\pi^+$ and $B_s^0 \to D_s^-K^+$ under the conditions of U-spin symmetry. It is shown that the analysis of time dependent decay rate asymmetries in $B_d^0 \to D^-\pi^+$ can result in a precision of $\sim 10^\circ$ on γ after five years of data taking under certain theoretical assumptions. The combined extraction of γ from the decay modes $B_d^0 \to D^-\pi^+$ and $B_s^0 \to D_s^-K^+$ is seen to allow an unambiguous extraction of γ, with a precision of $\sim 5^\circ$ after five years of data taking.

Contents

Table 1: A summary of the yields, purities, mistag (ω), mistag precision (σ_ω) , and tagging efficiency (ϵ_{tag}) in the channels $B_d^0 \to D^\mp\pi^\pm$ and $B_s^0 \to D_s^\mp K^\pm$, taken from [BNSVH07, Gli07]. The annual yield refers to 2fb^{-1} of data taking.

Decay Channel	Annual yield	B/S	ω	σ_ω (absolute, 2 fb^{-1})	ϵ_{tag}
$B_d^0 \to D^\mp\pi^\pm$	1340k	0.22	35%	1%	50%
$B_s^0 \to D_s^\mp K^\pm$	6.2k	0.7	30%	1%	60%

1 Introduction

One of the key physics goals of the LHCb experiment is to make a precise measurement of γ, currently the least well constrained [ea05b] angle in the CKM unitary triangle. The channels $B_d^0 \to D^\mp\pi^\pm$ and $B_s^0 \to D_s^\mp K^\pm$ allow for a theoretically clean extraction of γ, which is expected to be robust against new physics and thus provide a baseline measurement. Discrepancies between this determination of γ and measurements using strategies sensitive to new physics contributions will be a signature of non-Standard Model processes. The reconstruction of these channels at LHCb has been documented in [Gli07, BNSVH07], and the selection yields, purities, and expected tagging performance are given in Table 1. Yields are quoted in multiples of nominal LHCb running years, equivalent to 2fb^{-1} of data taking, throughout this document. The quoted tagging performance comes from a dedicated study [CLM07] carried out with the full LHCb Monte Carlo simulation.

The "conventional" extraction of γ from the channel $B_s^0 \to D_s^\mp K^\pm$, in which γ is extracted from a fit to the decay rate asymmetries between B_s^0 and $\overline{B_s^0}$ decaying to the same final state, has been documented in [CMR07]. Such an extraction is also possible for the channel $B_d^0 \to D^\mp\pi^\pm$. These measurements will, however, suffer from an ambiguity on the extracted value of γ. In general there will be an eightfold ambiguity, although this can be reduced to a twofold one in the case of $B_s^0 \to D_s^\mp K^\pm$ through the use of untagged events. Therefore, an alternative approach has been recently proposed [Fle03, Wil05], which exploits the U-spin symmetry between these decay modes and allows for an essentially unambiguous extraction of γ.

This note presents Monte Carlo studies performed to explore the viability of the conventional measurement of γ from the channel $B_d^0 \to D^\mp\pi^\pm$ at LHCb, as well as the viability of a U-spin analysis of the channels $B_d^0 \to D^\mp\pi^\pm$ and $B_s^0 \to D_s^\mp K^\pm$. The term "full Monte Carlo" will refer to Monte Carlo events generated using PYTHIA [SMS06] and processed with the full GEANT4 [All06] LHCb detector simulation. The term "toy Monte Carlo" will refer to Monte Carlo data containing only the B parameters relevant for the γ fit; the parameters for individual toy Monte Carlo events are generated from distributions measured on full Monte Carlo events.

The note is structured as follows: this section has motivated the study. Section 2 develops the mathematical formalism needed to describe CP violation in neutral B decays. Section 3 discusses the theoretical uncertainties associated with the "conventional" extraction of γ from the channel $B_d^0 \to D^\mp\pi^\pm$. Section 4 lists the current measurements of γ from this decay mode at the B factories. Section 5 introduces U-spin symmetry. Section 6 presents the "conventional" measurement of γ from the channel $B_d^0 \to D^\mp\pi^\pm$. Section 7 presents the measurement of γ from the channels $B_d^0 \to D^\mp\pi^\pm$ and $B_s^0 \to D_s^\mp K^\pm$ under conditions of U-spin symmetry. Section 8 discusses the prospects for a γ measurement at LHCb from these and related channels.

2 CP violation in neutral B decays

$B_{d,s}^0$ mesons produced at the LHC are created in one of two distinct flavour eigenstates

$$B_{d,s}^0 = \left(\overline{b}, [d,s]\right), \overline{B_{d,s}^0} = \left(b, \overline{[d,s]}\right), \tag{1}$$

however their propagation must be described using mass eigenstates which do not correspond to these flavour eigenstates. In particular, the mass eigenstates $|B_L\rangle$ and $|B_H\rangle$ can be written as a linear combination of the flavour eigenstates

$$|B_{L,H}\rangle = p\left|B^0_{d,s}\right\rangle \pm q\left|\overline{B^0_{d,s}}\right\rangle, \tag{2}$$

where $|p|^2 + |q|^2 = 1$. Since the CP operator transforms one flavour eigenstate into another, the mass eigenstates in the absence of CP violation are equivalent to the eigenstates of the CP operator.

CP violation in the decays $B^0_d \to D^{\mp}\pi^{\pm}$ and $B^0_s \to D^{\mp}_s K^{\pm}$, collectively written as $B^0_q \to D_q\overline{u}_q$, is measured from the rate asymmetries for the B^0_q and $\overline{B^0_q}$ mesons to decay into the same final state. These rate asymmetries can be parameterized as

$$A(t) \equiv \frac{\Gamma\left(B^0_q \to D_q\overline{u}_q\right)(t) - \Gamma\left(\overline{B}^0_q \to D_q\overline{u}_q\right)(t)}{\Gamma\left(B^0_q \to D_q\overline{u}_q\right)(t) + \Gamma\left(\overline{B}^0_q \to D_q\overline{u}_q\right)(t)} =$$
$$\frac{C\left(B^0_q \to D_q\overline{u}_q\right)\cos\left(\Delta M_q t\right) + S\left(B^0_q \to D_q\overline{u}_q\right)\sin\left(\Delta M_q t\right)}{\cosh\left(\Delta\Gamma_q t/2\right) - A_{\Delta\Gamma}\left(B_q \to D_q\overline{u}_q\right)\sinh\left(\Delta\Gamma_q t/2\right)}, \tag{3}$$

where q stands for the d or s quark, and u_q is a pion or kaon. ΔM_q is the mass difference between the B_L and B_H eigenstates in the B_q system. $\Delta\Gamma_q$ represents the decay width difference between the "heavy" and "light" B_q mass eigenstates, negligibly small for the B^0_d system. The terms which are relevant in the CP violation study are C,S, and $A_{\Delta\Gamma}$, referred to collectively as the CP-observables. They can be written as

$$C\left(B^0_q \to D_q\overline{u}_q\right) \equiv C_q = \frac{1 - |\xi_q|^2}{1 + |\xi_q|^2}; \tag{4}$$

$$S\left(B^0_q \to D_q\overline{u}_q\right) \equiv S_q = \frac{2\mathrm{Im}\left(\xi_q\right)}{1 + |\xi_q|^2}; \tag{5}$$

$$A_{\Delta\Gamma}\left(B^0_q \to D_q\overline{u}_q\right) = \frac{2\mathrm{Re}\left(\xi_q\right)}{1 + |\xi_q|^2}. \tag{6}$$

The dependence of these CP-observables on γ comes through the parameter ξ:

$$\xi_q = -\left(-1\right)^L e^{-i(\phi_q+\gamma)}\left[\frac{1}{x_q e^{i\delta_q}}\right]. \tag{7}$$

Here, ϕ_q is the mixing phase between B^0_q and $\overline{B}^0_q$, δ_q is a strong phase difference between the decay channels $\overline{B^0_q} \to D_q\overline{u}_q$ and $B^0_q \to D_q\overline{u}_q$ which is not CP-violating, and x_q represents the level of interference between the B^0_q and $\overline{B}^0_q$ decaying into the same final state. The term $\left(-1\right)^L$, where L is the angular momentum of the $D_q\overline{u}_q$ system, determines the sign of the sine term in the asymmetry. For the decays considered in this study, $L = 0$.

The parameter x_q can be thought of as the scale at which the decay $B^0_q \to D_q\overline{u}_q$ is sensitive to CP violation; the bigger x_q, the more sensitive the decay channel. The terms x_q and δ_q are related to the matrix elements M_q and $\overline{M}_q$, of the decays $\overline{B^0_q} \to D_q\overline{u_q}$ and $\overline{B^0_q} \to \overline{D_q}u_q$ respectively, through

$$a_q e^{i\delta_q} \propto \frac{M_q}{\overline{M}_q}, \tag{8}$$

where a_q is given by

$$a_s \equiv \frac{x_s}{R_b}, \tag{9}$$

$$a_d \equiv -\left(\frac{1-\lambda^2}{\lambda^2}\right)\frac{x_d}{R_b}, \tag{10}$$

and R_b is given by

$$R_b \equiv \left(1 - \frac{\lambda^2}{2}\right) \frac{1}{\lambda} \left|\frac{V_{ub}}{V_{cb}}\right|, \tag{11}$$

where $\lambda = 0.22$ is the sine of the Cabibbo angle, and $V_{ub,cb}$ are elements of the CKM matrix. There are analogous CP-observables for the other asymmetry, from a state B_q to $\overline{D}_q u_q$. These will be labelled $\overline{C}_q$,$\overline{S}_q$ and $\overline{A}_{\Delta\Gamma}$, but are governed by the same three equations above, with $\overline{\xi}_q$ replacing ξ_q:

$$\overline{\xi}_q = -(-1)^L e^{-i(\phi_q+\gamma)} \left[x_q e^{i\delta_q}\right]. \tag{12}$$

Finally, the CP-observables C and S can be written out explicitly in this notation:

$$C_q = -\left[\frac{1-x_q^2}{1+x_q^2}\right]; \tag{13}$$

$$\overline{C}_q = +\left[\frac{1-x_q^2}{1+x_q^2}\right]; \tag{14}$$

$$S_q = (-1)^L \left[\frac{2x_q \sin\left(\phi_q + \gamma + \delta_q\right)}{1+x_q^2}\right]; \tag{15}$$

$$\overline{S}_q = (-1)^L \left[\frac{2x_q \sin\left(\phi_q + \gamma - \delta_q\right)}{1+x_q^2}\right]. \tag{16}$$

3 Values of x_d and x_s

The sensitivity to γ in the decays $B_q^0 \to D_q \overline{u}_q$ depends on the expected interference between the tree level diagrams for a B_q^0 or $\overline{B}_q^0$ meson to decay into the same final state, parameterized by x_q. It is therefore important to determine the likely size of x_q.

A recent BaBar [ea08] analysis of the decays $B_d^0 \to D_s^{\mp}\pi^{\pm}$ has estimated x_d from the relation

$$x_d = \tan\left(\theta_C\right) \sqrt{\frac{B\left(B^0 \to D_s^+\pi^-\right)}{B\left(B^0 \to D_s^-\pi^+\right)}} \frac{f_D}{f_{D_s}}, \tag{17}$$

where θ_C is the Cabibbo angle, and the term $\frac{f_D}{f_{D_s}}$ is the ratio of decay constants for the D and D_s. The result is

$$x_d = 0.0175 \pm 0.0014\,(\mathrm{stat}) \pm 0.0009\,(\mathrm{syst}) \pm 0.0010\,(\mathrm{th}), \tag{18}$$

where the quoted theoretical error ($\sim 6\%$) comes from the assigned uncertainty on the knowledge [1)] of $\frac{f_D}{f_{D_s}}$ from lattice QCD. This does not, however account for the entire theoretical error on x_d, as acknowledged in the BaBar analysis: "Other SU(3) breaking effects are believed to affect [x_d] by (10-15) %". As discussed in [Baa07], the three major sources of theoretical uncertainty on x_d are rescattering diagrams, non-factorizable effects, and W-exchange amplitudes. The contribution from rescattering diagrams can be parameterized as a multiplicative correction factor R_i,

$$x_d = \tan\left(\theta_C\right) \sqrt{\frac{B\left(B^0 \to D_s^+\pi^-\right)}{B\left(B^0 \to D_s^-\pi^+\right)}} \frac{f_D}{f_{D_s}} R_i, \tag{19}$$

and the size of this factor can be calculated by fitting to the strong-interaction rescattering matrix. The uncertainty on this fit can be estimated by comparing the rescattered branching ratios for a variety of modes with the measured branching ratios. The theoretical error from the rescattering correction is 1%, and therefore negligible. The errors due to non-factorizable effects and W-exchange amplitudes are estimated at 9% (Gaussian) and 5% (flat) respectively. For the purpose of fitting to γ, it is necessary to calculate an overall error on x_d from the individual statistical,

1) Given the recent disagreement between theory and experiment regarding the value of f_{D_s}, this error is likely to increase.

systematic, and theoretical errors. The approach taken here will be to add these errors in quadrature, resulting in a total error of $\sigma_{x_d} \approx 20\%$. This error can, however, be expected to improve in the future. The statistical errors on the branching ratios will improve as more results are presented by the B-factories and LHCb, while the theoretical errors may be better understood by repeating the analysis of [Baa07] with more recent experimental inputs. By the time LHCb finishes taking data, it can be hoped that the value x_d will be known to better than 10%.

An analogous line of reasoning to that for x_d leads to an expected value of 0.37 for x_s, which has the significant advantage of being large enough to fit directly from the CP asymmetries in the channel $B_s^0 \to D_s^{\mp} K^{\pm}$. The precision with which this parameter will be measured is given in Table 5.

4 Current B factory measurements

Both BaBar [ea06b] and Belle [ea06c] have constrained $\sin(2\beta + \gamma)$ from the decay modes $B^0 \to D^{(*)\pm}\pi^{\mp}$, and in BaBar's case also from $B^0 \to D^{\pm}\rho^{\mp}$. BaBar places a combined constraint of $\sin(2\beta + \gamma) > 0.64\,(0.40)$ at the 68% (90%) confidence level. Belle places a constraint of $\sin(2\beta + \gamma) > 0.44\,(0.52)$ at the 68% confidence level from the $D^{*\pm}\pi^{\mp}$ ($D^{\pm}\pi^{\mp}$) modes.

5 U-spin symmetry

Since x_d cannot be fitted for, it will have to be externally constrained, and such constraints bring undesirable theoretical errors into the determination of γ. It is possible, however, to eliminate this parameter from the fits altogether by combining the analysis of the channels $B_d^0 \to D^{\mp}\pi^{\pm}$ with that of $B_s^0 \to D_s^{\mp} K^{\pm}$. This relies on U-spin symmetry, which is an SU(2) subgroup of the flavour SU(3) symmetry. Under U-spin symmetry, the (d,s) pair of quarks is a doublet, in a similar way to (u,d) under isospin. As an example of this mechanism, recall that under isospin, the pions are considered as isospin eigenstates of the same hadron

$$\pi^+\left(u\overline{d}\right) \equiv I_3 = +1; \tag{20}$$

$$\pi^0\left(u\overline{u} - d\overline{d}\right)/\sqrt{2} \equiv I_3 = 0; \tag{21}$$

$$\pi^-\left(\overline{u}d\right) \equiv I_3 = -1. \tag{22}$$

Although the I_3 component of isospin varies, $I = 1$ for all three pions. It is empirically observed that the strong interactions of the pions are almost identical. Since the three pions are related by the exchange of u and d quarks, isospin symmetry implies that strong interactions are unchanged under the exchange of u and d quarks. U-spin symmetry functions in the same way, but between d and s quarks. Hence the $B_s^0\,(b\overline{s})$ and $B_d^0\,\left(b\overline{d}\right)$ mesons, which are related by the exchange of a $\overline{d}$ quark for an $\overline{s}$ quark, are identical under U-spin, and their strong interactions are postulated to be identical also. In particular, parameters associated with the strong force, such as the phases $\delta_{d,s}$, have the same value for U-spin related decays.

U-spin is broken by the difference between the s and d quark masses, in the same way that isospin is broken by the difference between the d and u quark masses. Since the s quark is heavier than the u quark, U-spin breaking effects are greater than isospin breaking effects. On the other hand, there is no charge difference between the s and d quarks, so that U-spin symmetry, unlike isospin, is not broken by electroweak penguins. In addition, it has been argued in [SS07] that U-spin is expected to be a better symmetry than SU(3) when analyzing neutral B meson decays, because it does not require any assumptions about the relative amplitudes of different (tree, penguin, annihilation) decay topologies.

6 Conventional extraction of γ from $B_d^0 \to D^{\mp}\pi^{\pm}$

6.1 Fitting method

The angle γ can be extracted from the time dependent decay rate asymmetries introduced in Equation 3. An unbinned log-likelihood fit is performed to the asymmetries using ROOT [BR97] and the minimization package MINUIT [JR75]. The log-likelihood function to be maximized is

$$\ln L = \sum_{\text{all } B_d^0 \to D^-\pi^+} \ln\left(p_{S_d}(t_i)\right) + \sum_{\text{all } \overline{B}_d^0 \to D^-\pi^+} \ln\left(1 - p_{S_d}(t_i)\right) + \sum_{\text{all } \overline{B}_d^0 \to D^+\pi^-} \ln\left(p_{\overline{S}_d}(t_i)\right) + \sum_{\text{all } B_d^0 \to D^+\pi^-} \ln\left(1 - p_{\overline{S}_d}(t_i)\right). \quad (23)$$

$p_{S_d}(t_i)$ is the probability to find a $B_d^0 \to D^-\pi^+$ event at time t_i rather than a $\overline{B}_d^0 \to D^-\pi^+$ event, and $p_{\overline{S}_d}(t_i)$ is the probability to find a $\overline{B}_d^0 \to D^+\pi^-$ event at time t_i rather than a $B_d^0 \to D^+\pi^-$ event. In terms of the asymmetries defined in Equation 3, p_{S_d} and $p_{\overline{S}_d}$ are given by

$$p_{S_d,\overline{S}_d}(t) = \frac{A_{S_d,\overline{S}_d}(t) + 1}{2}. \quad (24)$$

In order to extract γ from the asymmetries, it is necessary to determine the value of C_d, S_d, and $\overline{S}_d$. However, C_d depends on x_d, and x_d is too small to fit for the decay channel $B_d^0 \to D^{\mp}\pi^{\pm}$; it will have to be determined from external sources. This uncertainty in the knowledge of x_d is accounted for by multiplying the likelihood function with a Gaussian

$$L_{\text{constrained}} = L \cdot e^{-\frac{\left(x_d^{\text{estim}} - x_d^{\text{fit}}\right)^2}{2\sigma_{x_d}^2}} \quad (25)$$

where x_d^{estim} is the assumed value of x_d as given by external sources, x_d^{fit} is the fit parameter, and σ_{x_d} is the uncertainty associated with x_d^{estim}.

6.2 Including detector effects

In order to add realism to the study, the following effects were considered

- Time resolution: The reconstructed decay time in this channel will be subject to an experimental resolution. The resolution measured in [Gli07] was a double Gaussian with a core resolution of 33 fs. For the sake of simplicity, however the resolution in this toy Monte Carlo study was modelled by a single Gaussian with a resolution of 40 fs.
- Acceptance function: The impact parameter and flight separation cuts used in the trigger and the offline channel selection will introduce a bias against events with a low B lifetime, referred to as a proper time acceptance.
- Mistag: The misidentification of B_d^0 mesons as $\overline{B}_d^0$ and vice versa dilutes the asymmetry. In the majority of time-dependent CP analyses, the mistag rate is determined from control channels, which can introduce systematic uncertainties in the fitting. In the case of $B_d^0 \to D^-\pi^+$, it will be shown that the mistag rate can be fitted from the asymmetries themselves, thus eliminating this potential source of error.
- Background: A background to signal level of $\frac{B}{S} = 0.22$ is assumed within a 3σ mass window (± 50 MeV), taken from the optimized selection in [Gli07].

These are now discussed in turn.

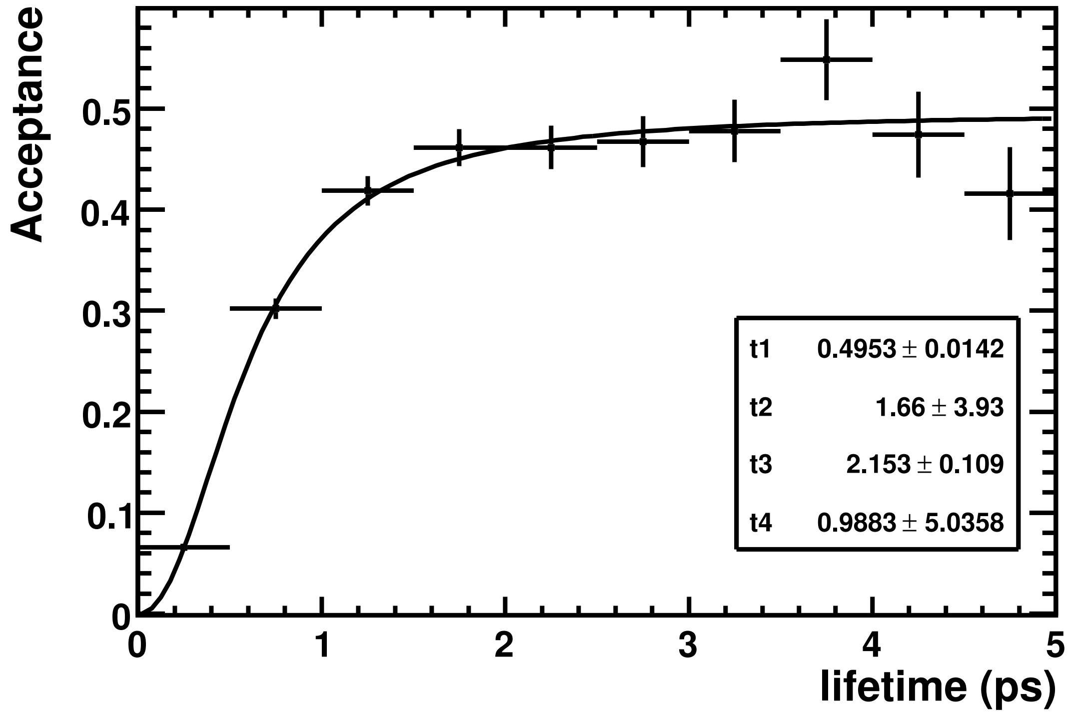

Figure 1: Fitted lifetime acceptance for signal $B_d^0 \to D^+\pi^-$ events passing the trigger and offline selection. The terms t1, t2, t3 and t4 correspond to the functional form $\frac{\mathrm{t1}\cdot\mathrm{t2}^{\mathrm{t3}}}{\mathrm{t4}+\mathrm{t2}^{\mathrm{t3}}}$

6.2.1 Time resolution

After an event has been generated, the time resolution is applied to its proper lifetime. If the smeared lifetime becomes negative, the event is discarded. During the fitting, the time resolution is ignored, enabling any systematic biases associated with it to be estimated.

6.2.2 Acceptance function

The acceptance function used to generate events in the toy Monte Carlo is taken from a fit to full Monte Carlo events as shown in Figure 1. The fitted function has the empirical form

$$P_A(t) = 0.5 \cdot \frac{(1.7t)^{2.2}}{1+(1.7t)^{2.2}}.$$

The acceptance function is not used when fitting, since it cancels out in the expression for the asymmetries. The overall normalization factor of 0.5 is a legacy of how this acceptance was calculated and does not affect the fit results.

6.2.3 Mistag

A mistag fraction ω will lead to B_d^0 mesons being wrongly identified as $\overline{B}_d^0$ mesons, and hence the decay rates for these two flavours of B^0 to decay into the same final state will be mixed together. Hence the apparent decay rate, $R_{\omega D^-}$, of the decays tagged as B_d^0 into $D^-\pi^+$ is given by

$$R_{\omega D^-}(t) = (1-\omega)R_{D^-}(t) + \omega\overline{R}_{D^-}(t), \tag{26}$$

and similarly for the other rates. The measured asymmetry is now diluted

$$A_\omega(t) = (1-2\omega)A(t), \tag{27}$$

compared to $A(t)$, the asymmetry for the case of perfect tagging.

6.2.4 Background

The background is assumed to be independent of the decay considered, so that a background $D^-\pi^+$ or $D^+\pi^-$ combination is equally likely to be identified as coming from a B_d^0 as it is to be identified as coming from a $\overline{B}_d^0$. It is assumed that the acceptance function will be the same for signal and background, and that the background will follow the $e^{-\Gamma t}$ distribution. These assumptions are justified by the fact that the major component of the background found in this channel [Gli07] are misidentified decays of B hadrons, which will have similar kinematics to the signal. In any case, the high purity of this channel means that the background is not likely to be a significant source of statistical error. Therefore, in the presence of a background to signal ratio of $\frac{B}{S}$, the apparent decay rate, $R_{\frac{B}{S}D^-}(t)$, of events tagged as B_d^0 into $D^-\pi^+$ is given by:

$$R_{\frac{B}{S}D^-}(t) = R_{D^-}(t) + \frac{B}{S} \cdot \frac{1}{2}\left(\overline{R}_{D^-}(t) + R_{D^-}(t)\right), \tag{28}$$

and similarly for the other rates. The measured asymmetry becomes

$$A_{\frac{B}{S}}(t) = \frac{1}{1+B/S} A(t). \tag{29}$$

6.3 The full asymmetry expression

The measured asymmetry now becomes

$$A_m(t) = \frac{1-2\omega}{1+B/S} A(t) = DA(t), \tag{30}$$

where $A(t)$ is again the asymmetry in the absence of any detector effects, and

$$D = \frac{1-2\omega}{1+B/S}, \tag{31}$$

represents the combined dilution of the asymmetry caused by the mistag and background.

Written out explicitly, using Equation 3, this is

$$A_m(t) = D\frac{C\left(B_q^0 \to D_q\overline{u}_q\right)\cos\left(\Delta M_q t\right) + S\left(B_q^0 \to D_q\overline{u}_q\right)\sin\left(\Delta M_q t\right)}{\cosh\left(\Delta\Gamma_q t/2\right) - A_{\Delta\Gamma}\left(B_q \to D_q\overline{u}_q\right)\sinh\left(\Delta\Gamma_q t/2\right)}, \tag{32}$$

and an analogous expression can be written down for $\overline{A}_m(t)$.

6.4 Fitting with detector effects included

In order to fit correctly in the presence of these detector effects, it is necessary to determine the background and mistag levels. The background is normally determined from the mass sidebands, and the mistag from control channels. In this case, the dilution due to detector effects, given by the ratio $\frac{1-2\omega}{1+B/S}$, can be fitted directly alongside the CP violating parameters, since the four decay rates provide four observables and x_d is constrained from external sources. It is not possible to fit S_d, $\overline{S}_d$, C_d, $\overline{C}_d$, x_d, and the dilution at the same time because the dilution would be maximally correlated with the sine and cosine terms in the asymmetry. Fixing the cosine terms (with x_d and its associated uncertainty as an input to the fit) allows the dilution to be disentangled from the magnitude of the sine term. In principle this means that the systematic errors associated with poor external knowledge of the mistag rate and a badly understood background under the mass peak can be avoided. Because $B_d^0 \to D^+\pi^-$ is expected to have a high purity, the background level was assumed to be well understood in this study, allowing the mistag rate to be fitted alongside $S_d, \overline{S}_d$.

Table 2: Values of parameters and constants used in the toy Monte Carlo.

Parameter	Value
ω	35%
x_d	0.0175
$\frac{S}{B}$	4.6
Δm	0.507 ps^{-1}
Γ	0.653 ps^{-1}
$P_A(t)$	measured on MC signal events

It is also possible to do the reverse, and fit to the background level in the circumstances where the mistag rate is well understood from external sources. Both approaches offer potential gains in other analyses. For example, comparing the background level under the peak as extrapolated from the sidebands to the fitted background level from the asymmetries could offer valuable hints on the presence of peaking background under the signal, which could cause a systematic bias in the fitted B_d^0 lifetime. If the mistag is sufficiently well understood from the control channels, it may be possible to divide the signal region in bins of mass, and fit to the background level in each bin separately from them, thus building the shape of the background without any recourse to Monte Carlo data. Alternatively, if the background level can be well understood through other means, a fit to the mistag may allow $B_d^0 \to D^-\pi^+$ to be used as a control channel for other channels with similar kinematics.

The final fit parameters chosen are[2)] $\left(\omega, x_d, S_d/x_d, \overline{S}_d/x_d\right)$. Table 2 lists the values of the various constants and parameters used as input in the toy simulation. For clarity, and since the two are trivially related, all precisions will be quoted on S_d, not S_d/x_d.

6.5 Precisions on the CP-observables and ω

The precision with which S_d and $\overline{S}_d$ are fitted is independent of their input values in the case where x_d is known perfectly. Imperfect knowledge of x_d introduces correlations between S_d and $\overline{S}_d$ which break this invariance. If σ_{S_d} is the uncorrelated error on S_d when x_d is perfectly known, the correlated error is given by

$$\sigma_{S_d}^{\text{corr}} = \sqrt{\left(\sigma_{S_d}\right)^2 + \left(S_d \frac{\sigma_{x_d}}{x_d}\right)^2}. \tag{33}$$

This error now depends on the input values of S_d and $\overline{S}_d$, and by extension γ, δ_d, and ϕ_d. Equation 33 has been empirically verified by comparing the results of log-likelihood fits performed with Equations 23 and 25. Instead of quoting $\left[\sigma_{S_d}, \sigma_{\overline{S}_d}\right]$ for a given $\left[S_d, \overline{S}_d, \sigma_{x_d}\right]$, only the uncorrelated errors will be quoted. The correlated error can then be computed for any given $\left[S_d, \overline{S}_d, \sigma_{x_d}\right]$ using Equation 33.

Table 3 summarises the expected precisions on the CP-observables $S_d, \overline{S}_d$, and ω after one and five years of data taking, for the case where the mistag is fitted, and where the mistag is fixed to its generator value. When fitting to the mistag, it is assumed that the background level is known exactly. This does not affect the precision on γ since the dilution, $\frac{1-2\omega}{1+B/S}$, could in any case have been fitted to instead, losing direct information on the mistag but preserving the precision on the CP-observables.

Fitting to the mistag causes a $\sim 7\%$ increase in $\left[\sigma_{S_d}, \sigma_{\overline{S}_d}\right]$. The error on ω is independent of the values of $\phi_d - \gamma$ and δ_d. After one year (2 fb^{-1}) it will be

$$\sigma_\omega = 0.1\%, \tag{34}$$

[2)] S_d/x_d are chosen instead of S_d in order to separate fully the CP-observables from the externally constrained term x_d in the fit.

Table 3: A summary of the expected statistical errors on the CP-observables $S_d, \overline{S}_d$, and ω in the channel $B_d^0 \to D^-\pi^+$, for one and five years of data taking, and where $\sigma_{x_d} = 0$. The relevant pull plots are unbiased in all cases, with a width of 1.

	ω	S_d	$\overline{S}_d$
σ_{1y}	0.1%	$1.05 \cdot 10^{-2}$	$1.05 \cdot 10^{-2}$
σ_{5y}	0.05%	$0.47 \cdot 10^{-2}$	$0.47 \cdot 10^{-2}$
σ_{1y} without fit to mistag	N/A	$0.98 \cdot 10^{-2}$	$0.98 \cdot 10^{-2}$
σ_{5y} without fit to mistag	N/A	$0.44 \cdot 10^{-2}$	$0.44 \cdot 10^{-2}$

and after five years (10 fb^{-1})

$$\sigma_\omega = 0.05\%. \tag{35}$$

The error on ω is also independent of the error on x_d. Although the nature of systematic errors associated with extracting the mistag with an imperfect knowledge of the background are unknown at present, the statistical precision is better than the expected precision from control channels quoted in Table 1.

6.6 Statistical error

The dependence of the statistical error on mistag, background, and the signal yield N_S is

$$\sigma_{S_d} \propto \frac{1}{1-2\omega}\sqrt{\frac{1+B/S}{N_S}}. \tag{36}$$

Furthermore, the lifetime acceptance biases the selection against low-lifetime events. These events are where the cosine terms in the asymmetries dominate, but the sensitivity to γ comes from the sine terms in the asymmetries, which are ordinarily small in magnitude compared to the cosine terms. It follows that the acceptance will reduce the difference in magnitudes between the sine and cosine terms in the asymmetries, and this is seen to improve the precision with which the parameters S_d and $\overline{S}_d$ can be fitted for a given number of events. The errors in the presence of the assumed acceptance function, relative to the errors when no acceptance function is present, are 10% smaller in the absence of mistag and background, and 30% smaller if mistag and background are included in the fit. If it is possible to achieve the same yield and purity using either lifetime-biasing or lifetime-unbiased cuts, for example with impact parameter rather than transverse momentum cuts, the selection using lifetime-biasing cuts will provide a B_d^0 sample with an intrinsically higher sensitivity to γ.

6.7 Systematic errors

Any systematic bias in the fitted value of a parameter can be shown on a pull plot, where the pull of observable x with fitted value x_{fit} and fitted error of σ_x is given by

$$\text{pull}_x = \frac{x - x_{\text{fit}}}{\sigma_x}. \tag{37}$$

For correctly fitted x, the pull plot should have a mean of 0 and a width of 1. A deviation from 0 in the mean indicates a systematic bias in the fitting, while a width different from 1 indicates that the fitting is not estimating the errors correctly. It is particularly interesting to consider possible systematic biases associated with the inclusion of the mistag rate as a free parameter in the fit, and the fact that the fit ignores resolution effects on the measured B lifetime.

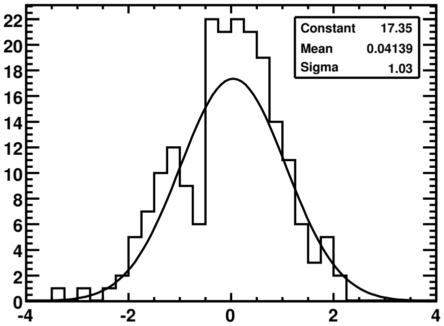

Figure 2: Pull plot on S_d when fitting with the mistag as a free parameter.

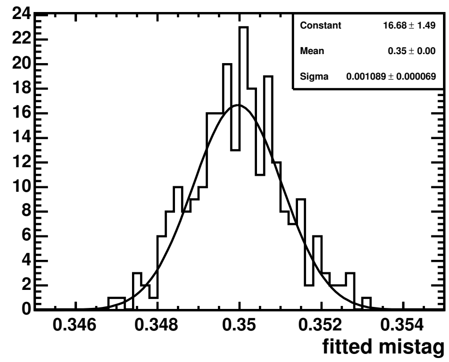

Figure 3: The value of the fitted mistag, for an input value of 0.35.

6.7.1 Mistag

Figure 2 shows the pull plots on the fitted parameter S_d in the case when the mistag is fitted, without any external input, from the asymmetries; the pull plots are clearly unbiased. Figure 3 shows the fitted value of the mistag. The one year precision on the value of the mistag of 0.1%, as given in Equation 34, underlines the potential of this channel to itself serve as a mistag control channel for other analyses. In the event that the background of this channel is poorly understood it is always possible to fit to the overall dilution instead, losing the mistag information while protecting against systematic errors on the extracted value of γ. Any asymmetry in the mistag rate of B^0 and $\overline{B^0}$ mesons will be determined from control channels.

6.7.2 Time resolution and acceptance function

The systematic error caused by ignoring the time resolution when fitting to the asymmetries is [Rad01] given by

$$\sigma_{syst,\sigma_t} \approx \frac{\Delta m \Gamma \sigma_\tau^2}{2x_d} \approx 1.0\%, \tag{38}$$

as a fraction of the fitted parameter itself. All detector effects were included in the pull study, and the value of x_d was assumed to be known exactly. The time resolution is introduced when generating the toy Monte Carlo, but no attempt is made to account for it when fitting, and the asymmetry fit is performed as if perfect proper time resolution were present. The mean value of the one year fit is biased by $(-0.06 \pm 0.04)\,\sigma_{1\mathrm{y}}$, while that of the five year fit is biased by $(-0.24 \pm 0.04)\,\sigma_{5\mathrm{y}}$, where $\sigma_{1\mathrm{y},5\mathrm{y}}$ is the appropriate statistical error. Since the statistical error decreases after five years of data taking, it is expected that the bias will increase as a fraction of the statistical error, and the results are consistent with a constant absolute bias due to the time resolution. The systematic error resulting from ignoring the time resolution in the fits will therefore not be negligible when compared to the statistical error on S_d and $\overline{S}_d$.

It is in principle possible to account for the presence of time resolutions in the fit[3)], which will reduce any observed bias. Also, it is empirically observed that the bias due to the time resolution is reduced by approximately a factor of 2 in the absence of an acceptance function.

A bias of around one fifth of the statistical precision on S_d will propagate into an equivalent bias on the value of γ.

6.8 Ambiguities in the extracted value of γ

In order to extract γ from the CP asymmetries given the measured values of the CP-observables, it is necessary to eliminate the hadronic phase, δ_q, from the equations for the CP-observables $S_d, \overline{S}_d$.

[3)] See, for example, a similar fit in the channel $B_s^0 \to D_s^\mp K^\pm$ [CMR07].

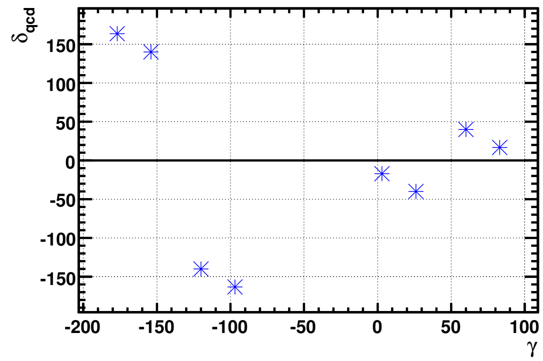

Figure 4: A plot of the ambiguous solutions for γ and δ_d for true $\gamma = 60°$ and $\delta_d = 40°$. Note that $\delta_{qcd} \equiv \delta_d$ on the vertical axis.

Table 4: A list of the ambiguous solutions for γ and δ_d, in the case when the "true" values are $\gamma = 60°$ and $\delta_d = 40°$.

γ	$-177°$	$-154°$	$-120°$	$-97°$	$3°$	$26°$	$60°$	$83°$
δ_d	$163.5°$	$140°$	$-140°$	$-163°$	$-17°$	$-40°$	$40°$	$17°$

It will be advantageous to define orthogonal combinations of the CP-observables $C, \overline{C}, S_d, \overline{S}_d$

$$\begin{aligned}
\langle C_q \rangle_+ &\equiv \frac{\overline{C}_q + C_q}{2} = 0; \\
\langle C_q \rangle_- &\equiv \frac{\overline{C}_q - C_q}{2} = \frac{1 - x_q^2}{1 + x_q^2}; \\
\langle S_q \rangle_+ &\equiv \frac{\overline{S}_q + S_q}{2} = +(-1)^L \left[\frac{2x_q \cos\delta_q}{1 + x_q^2}\right] \sin(\phi_q + \gamma); \\
\langle S_q \rangle_- &\equiv \frac{\overline{S}_q - S_q}{2} = -(-1)^L \left[\frac{2x_q \sin\delta_q}{1 + x_q^2}\right] \cos(\phi_q + \gamma).
\end{aligned} \tag{39}$$

The term $\sin(\phi_d - \gamma)$ can now be extracted from

$$\sin(\phi_d - \gamma)^2 = \frac{1}{2}\left[\left(1 + \langle S_d \rangle_-^2 - \langle S_d \rangle_+^2\right) \pm \sqrt{\left(1 + \langle S_d \rangle_-^2 - \langle S_d \rangle_+^2\right) - 4\langle S_d \rangle_-^2}\right]. \tag{40}$$

Hence the formula corresponds to a fourfold solution for $\sin(\phi_d - \gamma)$, and therefore an eightfold solution for γ itself. Because ϕ_d is known to such a high precision [ea06a] a measurement of $\phi_d - \gamma$ can be interpreted as a measurement of γ. Figure 4 shows the situation for an input value of $\gamma = 60°$, $\delta_d = 40°$, with the ambiguous solutions for γ and δ_d listed in Table 4. Notice that the γ values associated with some of the solutions are too close to be resolved without external knowledge of δ_d, or a precision on each individual solution of less than $10°$. Such degenerate solutions lead to a greater error on γ than that associated with each individual solution.

6.9 Precision on γ

It is now time to calculate an expected precision on γ from the precisions on the CP-observables quoted in Table 3. This is done by drawing contour plots in δ_d - γ space which are then projected onto the γ axis. It is desirable to develop a procedure which can be used when the actual fit is eventually performed with real data. It is assumed that a fit has been performed to the CP asymmetries; the fitted values of the CP-observables, their uncertainties, and σ_{x_d} are the inputs from which a precision on γ is computed. The following procedure is used:

1. The starting point are the values of the CP-observables and their uncertainties, obtained from a fit to the CP asymmetries, and σ_{x_d}. These will be referred to as the "measured" CP-observables.
2. The CP-observables $S_d, \overline{S}_d$ corresponding to each point in δ_d - γ space are calculated.
3. For each point, Equation 33 is used to calculate the correlated errors on the CP-observables.
4. 100 toy experiments are generated using the correlated errors for each point in δ_d - γ space. Each toy experiment gives "fitted" values of $S_d, \overline{S}_d$, whose Gaussian separation from the measured values is computed. This results in two constraints on the values of γ and δ_d, one corresponding to S_d and one corresponding to $\overline{S}_d$.
5. The constraints for $S_d, \overline{S}_d$ are multiplied together to obtain the overall constraint in δ_d - γ space for a given measured value of S_d,$\overline{S}_d$, and σ_{x_d}.
6. The overall PDF is then projected onto the γ axis.

The final result is a likelihood plot in γ, from which the 1σ, 2σ, etc. precisions on γ can be calculated. This procedure will now be illustrated for two interesting values of γ and δ_d. In both cases, σ_{x_d} is assumed to be 20% after one year of data taking, and 10% after five. Also, it is assumed that ϕ_d is known exactly.

6.9.1 $\gamma = 60°$ and $\delta_d = 10°$

The first scenario corresponds to the factorization limit, in which the strong phase δ_d is small. The contour plots after one year of data taking are shown in Figure 5, with the final γ likelihood in the bottom right hand corner. As can be seen, the eight ambiguous solutions group together in two areas of parameter space, each containing four solutions which are statistically indistinguishable. The central value of γ suffers from a large bias ($\sim 20°$). Looking at the combined contour plot in the bottom left of Figure 5, it is clear that this bias is caused by the near degeneracy in γ of two of the "fake" solutions around 40°.

The contour plots after five years of data taking are shown in Figure 6. The bias has been reduced, and looking at the combined constraint plot it can be seen that the degenerate solutions are beginning to be statistically separated from each other. Quoting a central value and error on γ is futile in this situation, but the likelihood can still contribute to the global knowledge on γ when combined with other measurements which do not suffer from the same degeneracy problems (for example measurements of γ from $B^{\pm} \to D^0 K^{\pm}$ techniques).

6.9.2 $\gamma = 60°$ and $\delta_d = 60°$

Since the value of δ_d is not constrained by any existing data, it is interesting to explore the achievable precision on γ in the case of a larger δ_d. As will be discussed in Section 7.1, sizeable non-factorizable effects could exist which lead to such a scenario.

The contour plots after one year of data taking are shown in Figure 7, with the final γ likelihood in the bottom right hand corner. The eight ambiguous solutions are still grouped in two bunches of four, but the individual solutions within each foursome are now close to being statistically distinguishable. The contour plots after five years of data taking are shown in Figure 8. The eight individual solutions are now clearly visible, although their statistical separation is still only around 1σ. Once again, the most useful way in which this measurement would contribute to the global knowledge of γ is by being combined with measurements which do not suffer from degeneracy problems.

6.10 Introducing information from $B_s^0 \to D_s^- K^+$

The ambiguous solutions are a problem not only because of their number, but also because of their degeneracy. One way to break this degeneracy is to introduce assumptions about the value of δ_d. Anticipating the eventual combined analysis of these channels in Section 7, U-spin symmetry can be used to related δ_d to δ_s

$$\delta_d = \delta_s, \tag{41}$$

which will be measured along with γ from $B_s^0 \to D_s^- K^+$. The errors on this equality will come from the statistical error on δ_s and U-spin breaking effects. The statistical error on γ from $B_s^0 \to D_s^- K^+$ is expected to be $\sim 10^\circ$ after one year [CMR07], and if this extraction is unambiguous then δ_s will be known with the same precision. This error will be doubled to account for U-spin breaking effects; this is a conservative assumption, particularly if δ_s is small. Therefore the precisions with which δ_d is known will be taken as

$$\sigma_{\delta_d}^{1\text{y}} = 20^\circ;$$

$$\sigma_{\delta_d}^{5\text{y}} = 10^\circ.$$

In both cases, the knowledge of δ_d is implemented as a Gaussian constraint on the contours in δ_d - γ space before projecting onto the γ axis.

6.10.1 $\gamma = 60^\circ$ and $\delta_d = 10^\circ$

The contour plots after one year of data taking are shown in Figure 9, and the bias in γ is still present, although the second foursome of ambiguous solutions has been ruled out. After five years, however, the "correct" value of γ is beginning to be better isolated, as seen in Figure 10. It is now useful to quote a precision on γ

$$\gamma_{5\text{y}} = \left(56^{+22}_{-41}\right)^\circ,$$

and the upper limit may usefully contribute to the world average.

6.10.2 $\gamma = 60^\circ$ and $\delta_d = 60^\circ$

The contour plots after one year of data taking are shown in Figure 11, and the "correct" solution for γ is already well separated from the remaining ambiguous solution. The measured value of γ is

$$\gamma_{1\text{y}} = \left(60^{+30}_{-21}\right)^\circ.$$

The contour plots after five years are shown in Figure 12. All ambiguous solutions have been ruled out, and the measured value of γ is

$$\gamma_{5\text{y}} = \left(60^{+11}_{-10}\right)^\circ.$$

6.11 Summary of conventional extraction

The angle γ can be extracted with a precision which depends significantly on the values of the parameters δ_d and $\phi_d - \gamma$. The value of the mistag can be fitted from the asymmetries independently of any external information about its value, which eliminates one significant source of systematic error in the fit. The achievable precision on γ depends on the lifetime distribution of the selected B_d^0 mesons, with samples richer in longer lived B_d^0 particles affording a better sensitivity to γ. The precision achievable on the value of γ depends significantly on the knowledge of the parameter x_d, which must be established from external sources.

The "conventional" extraction of γ suffers from an eightfold ambiguity on the extracted value of γ, which also decreases the precision on γ because some of the ambiguous solutions are degenerate. In the limit of small δ_d, these degeneracies prevent the "correct" value of γ from being isolated even after 5 years of data taking, unless information from $B_s^0 \to D_s^- K^+$ is introduced to constrain the value of δ_d and break the degeneracy. The bigger the strong phases, the easier these degenerate

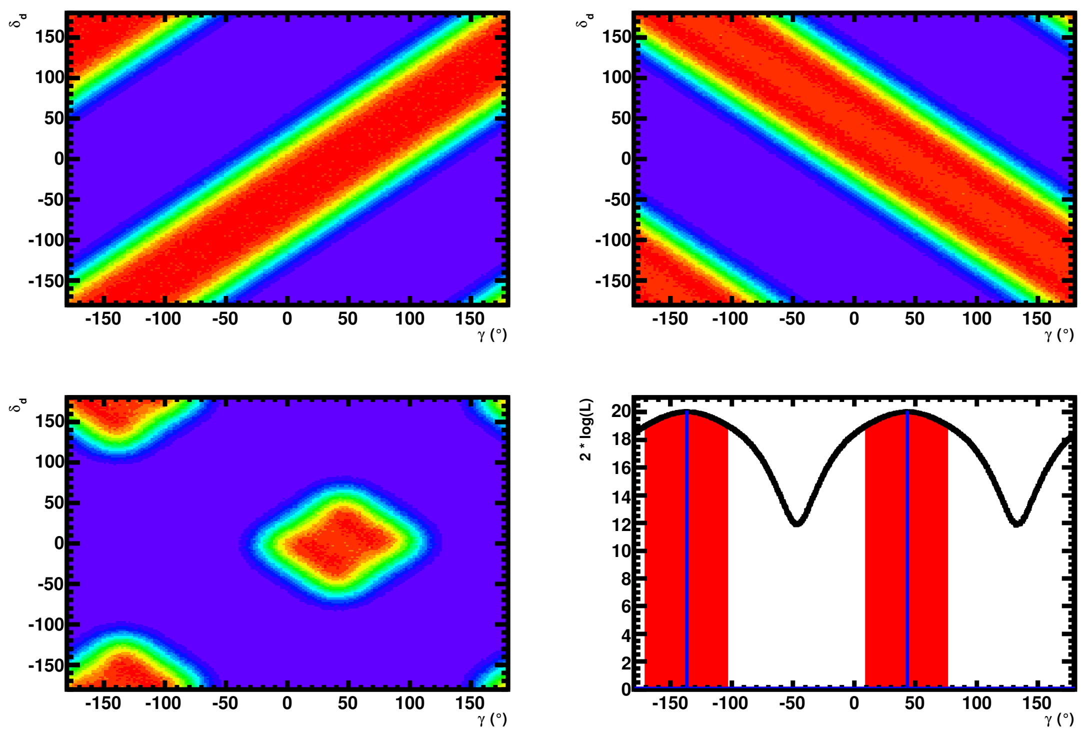

Figure 5: Contour plots showing the constraints in the δ_d - γ plane from S_d (top left), $\overline{S}_d$ (top right), and the combined constraint from S_d and $\overline{S}_d$ (bottom left). The likelihood projection in γ is shown in the bottom right plot. Warmer colours indicate a greater probability density. The blue line(s) correspond to the central value(s) for γ, while the red area indicates the 1σ interval corresponding to the central value(s). This plot is made with input values of $\gamma = 60^\circ$, $\delta_d = 10^\circ$, one year of data taking, and a 20% uncertainy on the assumed value of $x_d = 0.0175$. No constraint is applied on δ_d when calculating the likelihood. Note that the units of δ_d on the vertical axis are degrees.

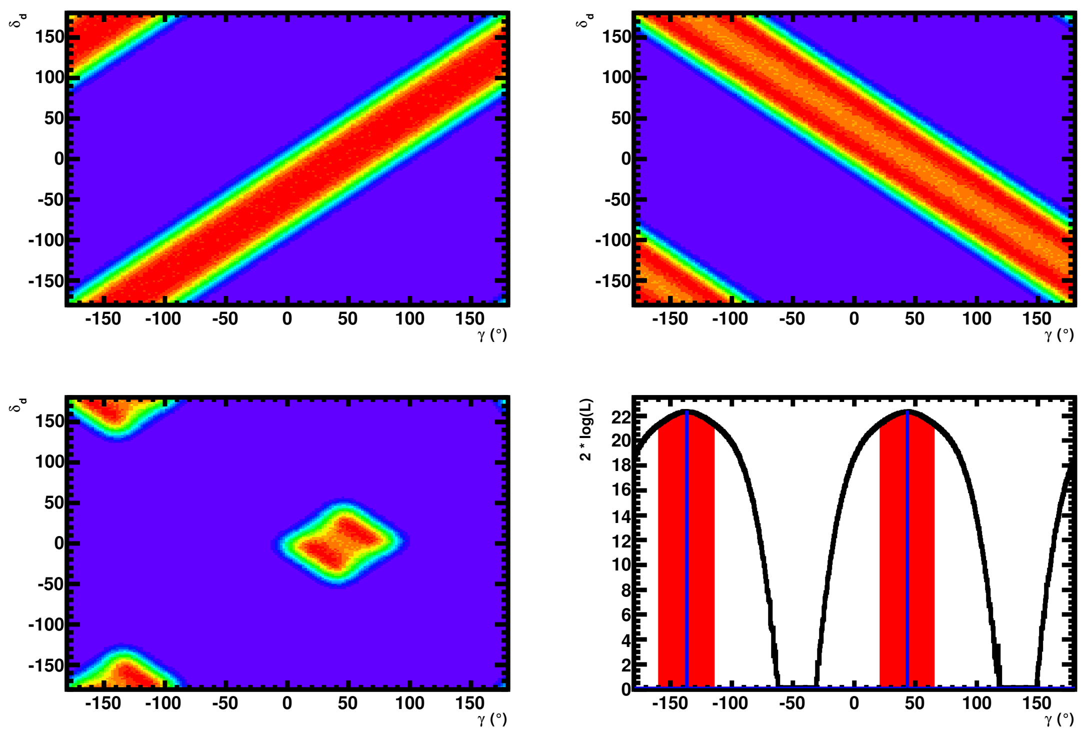

Figure 6: Contour plots showing the constraints in the δ_d - γ plane from S_d (top left), $\overline{S}_d$ (top right), and the combined constraint from S_d and $\overline{S}_d$ (bottom left). The likelihood projection in γ is shown in the bottom right plot. Warmer colours indicate a greater probability density. The blue line(s) correspond to the central value(s) for γ, while the red area indicates the 1σ interval corresponding to the central value(s). This plot is made with input values of $\gamma = 60^{\circ}$, $\delta_d = 10^{\circ}$, five years of data taking, and a 10% uncertainy on the assumed value of $x_d = 0.0175$. No constraint is applied on δ_d when calculating the likelihood. Note that the units of δ_d on the vertical axis are degrees.

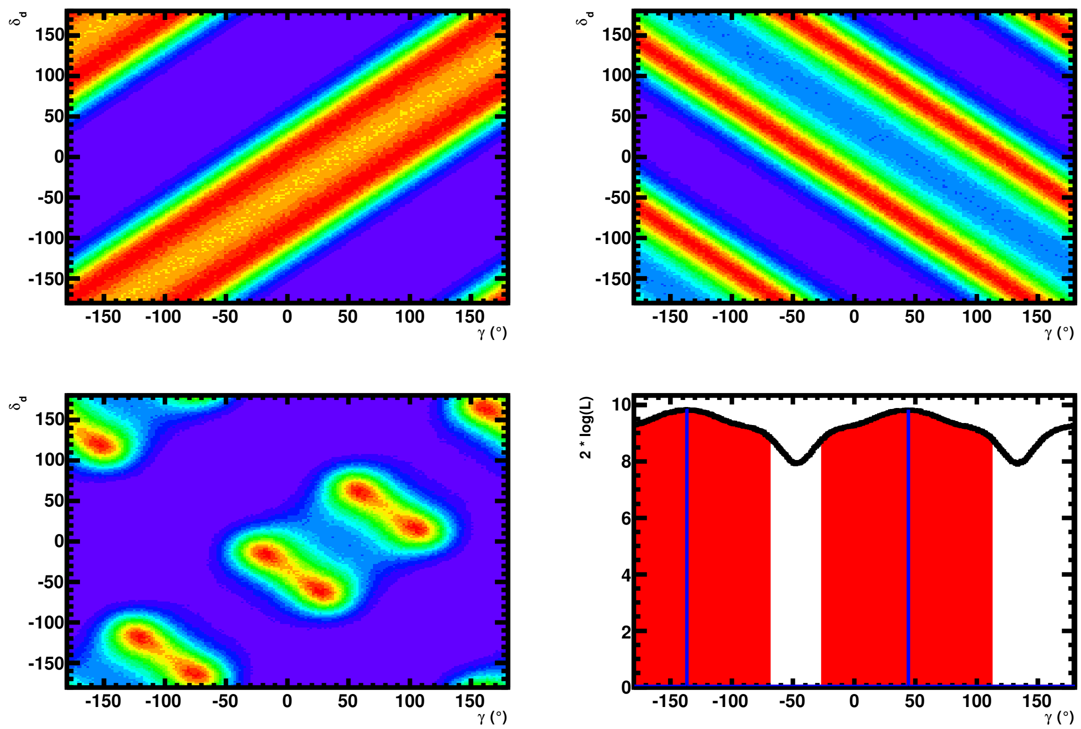

Figure 7: Contour plots showing the constraints in the δ_d - γ plane from S_d (top left), $\overline{S}_d$ (top right), and the combined constraint from S_d and $\overline{S}_d$ (bottom left). The likelihood projection in γ is shown in the bottom right plot. Warmer colours indicate a greater probability density. The blue line(s) correspond to the central value(s) for γ, while the red area indicates the 1σ interval corresponding to the central value(s). This plot is made with input values of $\gamma = 60°$, $\delta_d = 60°$, one year of data taking, and a 20% uncertainy on the assumed value of $x_d = 0.0175$. No constraint is applied on δ_d when calculating the likelihood. Note that the units of δ_d on the vertical axis are degrees.

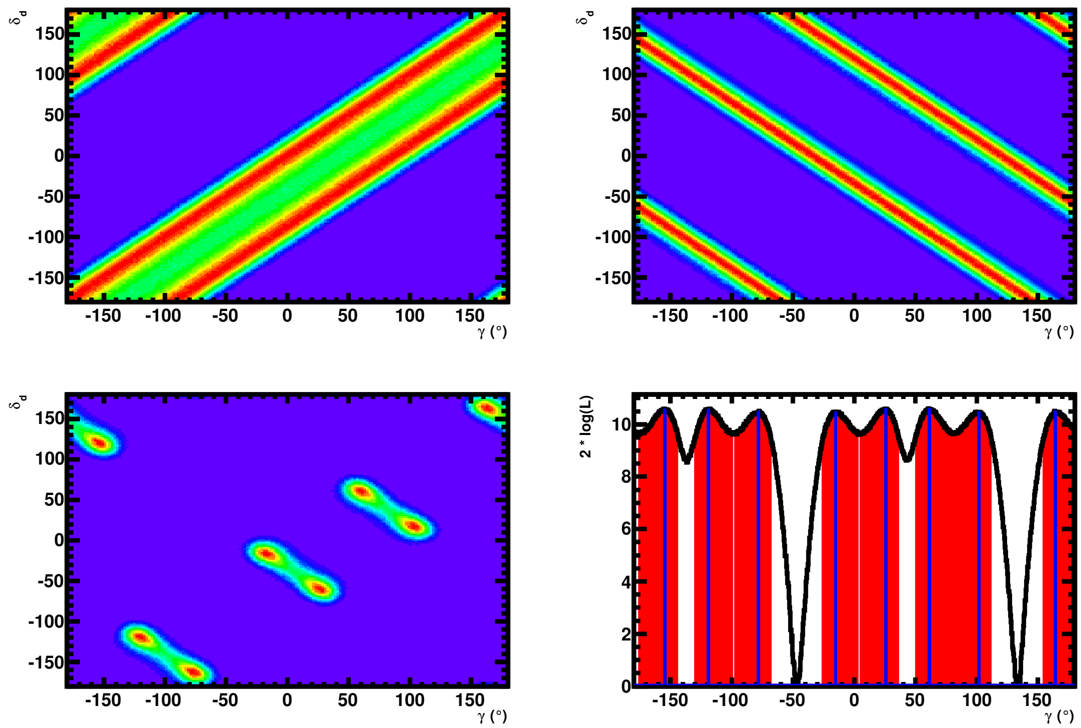

Figure 8: Contour plots showing the constraints in the δ_d - γ plane from S_d (top left), $\overline{S}_d$ (top right), and the combined constraint from S_d and $\overline{S}_d$ (bottom left). The likelihood projection in γ is shown in the bottom right plot. Warmer colours indicate a greater probability density. The blue line(s) correspond to the central value(s) for γ, while the red area indicates the 1σ interval corresponding to the central value(s). This plot is made with input values of $\gamma = 60^{\circ}$, $\delta_d = 60^{\circ}$, five years of data taking, and a 10% uncertainy on the assumed value of $x_d = 0.0175$. No constraint is applied on δ_d when calculating the likelihood. Note that the units of δ_d on the vertical axis are degrees.

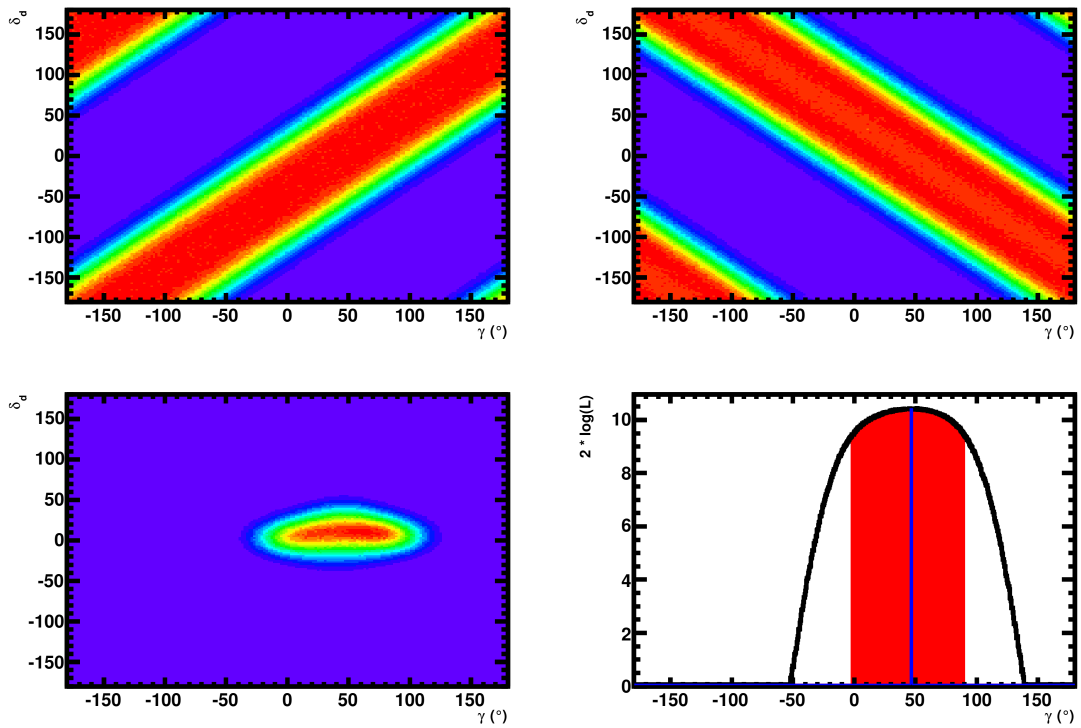

Figure 9: Contour plots showing the constraints in the δ_d - γ plane from S_d (top left), $\overline{S}_d$ (top right), and the combined constraint from S_d and $\overline{S}_d$ (bottom left). The likelihood projection in γ is shown in the bottom right plot. Warmer colours indicate a greater probability density. The blue line(s) correspond to the central value(s) for γ, while the red area indicates the 1σ interval corresponding to the central value(s). This plot is made with input values of $\gamma = 60^\circ$, $\delta_d = 10^\circ$, one year of data taking, and a 20% uncertainty on the assumed value of $x_d = 0.0175$. A Gaussian constraint of $\delta_d = (10 \pm 20)^\circ$ is applied on δ_d when calculating the likelihood. Note that the units of δ_d on the vertical axis are degrees.

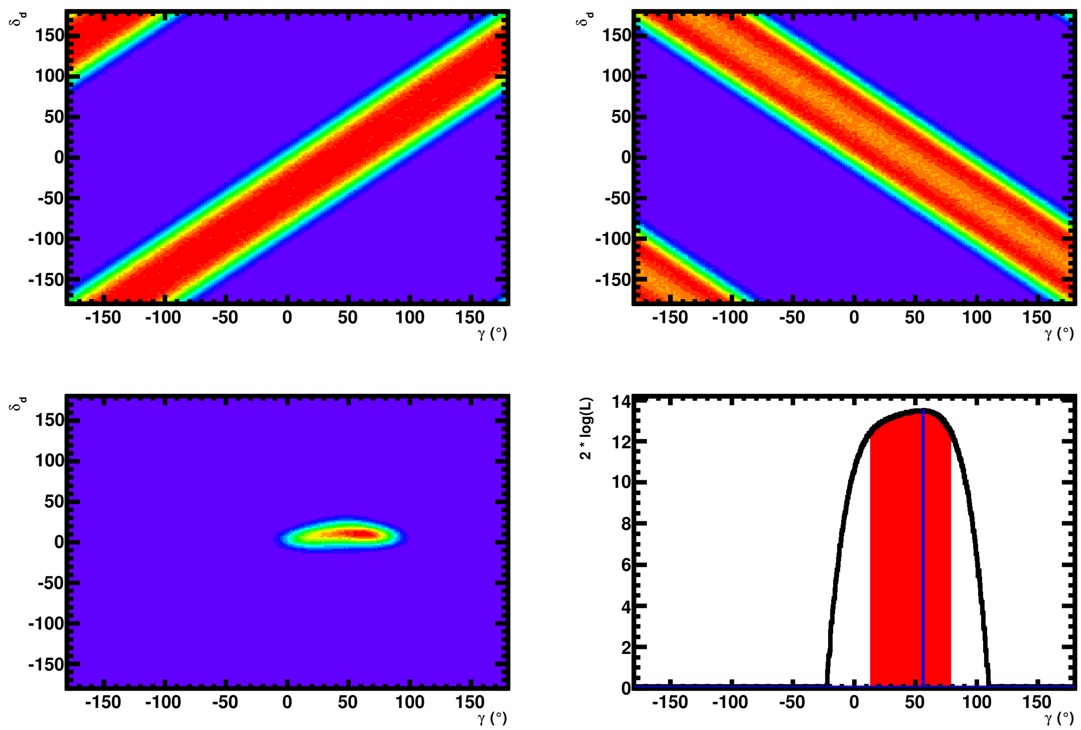

Figure 10: Contour plots showing the constraints in the δ_d - γ plane from S_d (top left), $\overline{S}_d$ (top right), and the combined constraint from S_d and $\overline{S}_d$ (bottom left). The likelihood projection in γ is shown in the bottom right plot. Warmer colours indicate a greater probability density. The blue line(s) correspond to the central value(s) for γ, while the red area indicates the 1σ interval corresponding to the central value(s). This plot is made with input values of $\gamma = 60^\circ$, $\delta_d = 10^\circ$, five years of data taking, and a 10% uncertainy on the assumed value of $x_d = 0.0175$. A Gaussian constraint of $\delta_d = (10 \pm 10)^\circ$ is applied on δ_d when calculating the likelihood. Note that the units of δ_d on the vertical axis are degrees.

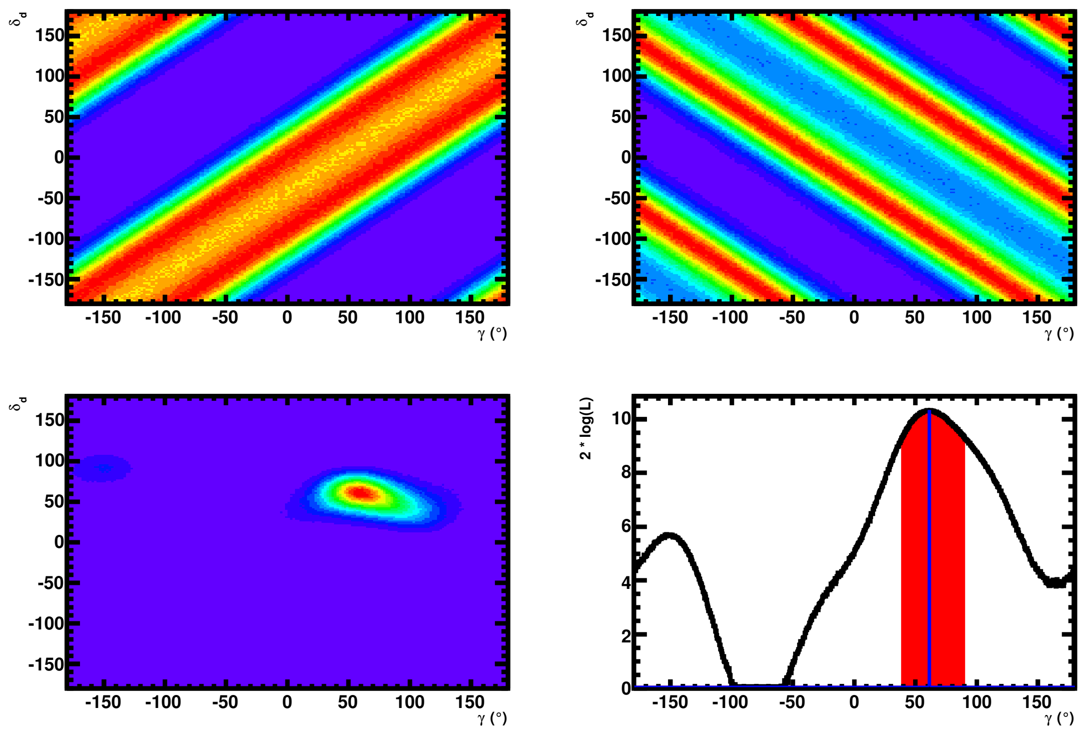

Figure 11: Contour plots showing the constraints in the δ_d - γ plane from S_d (top left), $\overline{S}_d$ (top right), and the combined constraint from S_d and $\overline{S}_d$ (bottom left). The likelihood projection in γ is shown in the bottom right plot. Warmer colours indicate a greater probability density. The blue line(s) correspond to the central value(s) for γ, while the red area indicates the 1σ interval corresponding to the central value(s). This plot is made with input values of $\gamma = 60^\circ$, $\delta_d = 60^\circ$, one year of data taking, and a 20% uncertainy on the assumed value of $x_d = 0.0175$. A Gaussian constraint of $\delta_d = (60 \pm 20)^\circ$ is applied on δ_d when calculating the likelihood. Note that the units of δ_d on the vertical axis are degrees.

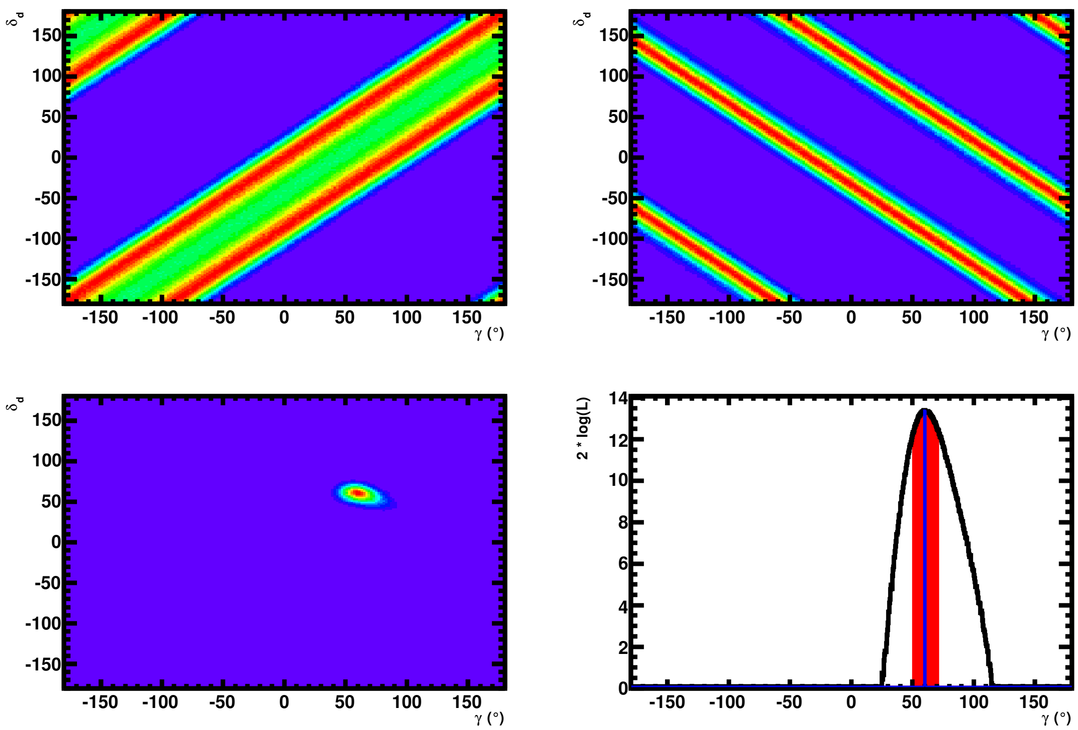

Figure 12: Contour plots showing the constraints in the δ_d - γ plane from S_d (top left), $\overline{S}_d$ (top right), and the combined constraint from S_d and $\overline{S}_d$ (bottom left). The likelihood projection in γ is shown in the bottom right plot. Warmer colours indicate a greater probability density. The blue line(s) correspond to the central value(s) for γ, while the red area indicates the 1σ interval corresponding to the central value(s). This plot is made with input values of $\gamma = 60^\circ$, $\delta_d = 60^\circ$, five years of data taking, and a 10% uncertainy on the assumed value of $x_d = 0.0175$. A Gaussian constraint of $\delta_d = (60 \pm 10)^\circ$ is applied on δ_d when calculating the likelihood. Note that the units of δ_d on the vertical axis are degrees.

solutions are to separate, but external input on the value of δ_d is still required to extract a single solution for γ.

An alternative method for extracting γ, which resolves the ambiguous solutions as well as requiring no *a priori* knowledge of the parameter x_d, is now presented.

7 Extraction of the angle γ through the U-spin analysis of the channels $B_d^0 \to D^- \pi^+$ and $B_s^0 \to D_s^- K^+$

The last section showed that the conventional extraction of γ from the channel $B_d^0 \to D^- \pi^+$ suffers from two weaknesses which complicate the extraction of γ:

1. An eightfold ambiguity on the extracted value of γ;
2. The requirement that x_d is well constrained from external sources.

This section will discuss a method of measuring γ by using the U-spin symmetry between the channels $B_d^0 \to D^- \pi^+$ and $B_s^0 \to D_s^- K^+$, proposed in [Fle03], which offers the potential for an unambiguous extraction of γ and does not require any knowledge of x_d. Before discussing the full combined extraction, however, two ways on reducing the number of ambiguous solutions for γ in each individual channel are described.

7.1 Reducing the ambiguity through factorization

One technique for eliminating ambiguous solutions is to use factorization arguments. Here they can be used to fix the sign of $\cos \delta_q$ in Equation 39, thus enabling the sign of $\sin(\phi_q + \gamma)$ to be fixed. Factorizing the four-quark matrix operators $M_q, \overline{M}_q$ in Equation 8 into the product of two quark currents allows the sign of their ratio to be determined, which in turn allows the sign of δ_q and therefore $\sin(\phi_q + \gamma)$ to be determined. The details of the calculation are given in [Fle03], and the result is (for the modes with $L = 0$)

$$\delta_q|_{\text{fact}} = 0^\circ. \tag{42}$$

Hence the sign of $\sin(\phi_q + \gamma)$ is seen to be positive, reducing the number of ambiguous solutions by half. It should be noted that the factorization assumption may receive sizable corrections for $\overline{B_q^0} \to \overline{D_q} u_q$ decays, where the spectator quark q ends up in the "light" u_q meson. Nonetheless, it is expected that these corrections will not change the sign of $\cos \delta_q$.

7.2 Exploiting $A_{\Delta\Gamma}$

There is another observable yet to be exploited in Equation 3, $A_{\Delta\Gamma}$:

$$A_{\Delta\Gamma} = \frac{2\text{Re}\xi_q}{1 + |\xi_q|^2}. \tag{43}$$

Within the asymmetry, $A_{\Delta\Gamma}$ is multiplied by the term $\sinh(\Delta\Gamma_q t/2)$, where $\Delta\Gamma_q$ is the width difference of the B_q mass eigenstate. This width is negligible in the B_d^0 sector, however, it may play a substantial role in the B_s sector, where $\Delta\Gamma_q/\Gamma_q$ has been determined at the Tevatron [ea05a, ea07] as $|\Delta\Gamma_q/\Gamma_q| \sim 10\%$. It is therefore worth briefly reviewing its importance with respect to the decay $B_s^0 \to D_s^- K^+$, with reference to the latest LHCb Monte Carlo studies in this channel [CMR07].

What makes $A_{\Delta\Gamma}$ such a useful observable is that it can be extracted from the untagged rate $\Gamma\left(B_q^0\left(t\right) \to D_q\overline{u}_q\right)$, i.e. the combined rate for B_q^0 and $\overline{B_q^0}$ events to decay into the same final state

$$\Gamma\left(B_q^0 \to D_q\overline{u}_q\right)(t) = \left[\Gamma\left(B_q^0 \to D_q\overline{u}_q\right) + \Gamma\left(\overline{B_q^0} \to D_q\overline{u}_q\right)\right] \times \left[\cosh\left(\Delta\Gamma_q t/2\right) - A_{\Delta\Gamma}\sinh\left(\Delta\Gamma_q t/2\right)\right] e^{-\Gamma_q t}. \quad (44)$$

Here, Γ_q refers to the average decay width, $\Gamma_q = \left(\Gamma_H^q + \Gamma_L^q\right)/2$. This provides valuable information on γ through the constraint

$$[C]^2 + [S]^2 + [A_{\Delta\Gamma}]^2 = 1, \quad (45)$$

The fact that $A_{\Delta\Gamma}$ has a qualitatively different dependence on γ than C or S allows this relation to be used to eliminate certain ambiguities in the extracted value of γ. The inclusion of untagged events also substantially increases the number of events available to the analysis, since the tagging power in B_s channels is only expected to be around 8%. It has been shown that including these untagged events in the study improves the precision with which $\gamma + \phi_s$ can be measured in the channel $B_s^0 \to D_s^- K^+$ from $\sim 12^\circ$ to $\sim 10^\circ$ in 1 year of LHCb running in a conventional analysis. In the context of the combined U-spin analysis, using untagged events results in an improved precision on the parameters $S_s, \overline{S}_s$.

7.3 Combined extraction of γ

The combined extraction of γ relies on the U-spin symmetry between the channels $B_d \to D_d\overline{u}_d$ and $B_s \to D_s\overline{u}_s$, which are obtained by replacing all down quarks in the decay by strange quarks. From Equation 39 it follows that

$$\left[\frac{a_s\cos\delta_s}{a_d\cos\delta_d}\right] R = -\left(-1\right)^{L_s - L_d}\left[\frac{\sin\left(\phi_d+\gamma\right)}{\sin\left(\phi_s+\gamma\right)}\right]\left[\frac{\langle S_s\rangle_+}{\langle S_d\rangle_+}\right], \quad (46)$$

and similarly

$$\left[\frac{a_s\sin\delta_s}{a_d\sin\delta_d}\right] R = -\left(-1\right)^{L_s - L_d}\left[\frac{\cos\left(\phi_d+\gamma\right)}{\cos\left(\phi_s+\gamma\right)}\right]\left[\frac{\langle S_s\rangle_-}{\langle S_d\rangle_-}\right], \quad (47)$$

where

$$R \equiv \left(\frac{1-\lambda^2}{\lambda^2}\right)\left[\frac{1+x_d^2}{1+x_s^2}\right]. \quad (48)$$

Here, λ is the sine of the Cabibbo angle. For the decays considered here, $L_s = L_d = 0$, and exact U-spin symmetry implies that

$$a_s = a_d, \ \delta_s = \delta_d. \quad (49)$$

Substituting these into Equations 46 and 47, it is possible to extract γ unambiguously in a number of ways, depending on what additional assumptions are made. Three scenarios are considered in turn: a strong U-spin assumption, a phase U-spin assumption, and an amplitude U-spin assumption.

7.3.1 Strong U-spin assumption

In this scenario, it is assumed that $\delta_s = \delta_d$ and $a_s = a_d$. Equations 46 and 47 are used to constrain γ, and their theoretical uncertainties are determined by U-spin breaking corrections to

$$a_s\cos\left(\delta_s\right) = a_d\cos\left(\delta_d\right),$$

and

$$a_s\sin\left(\delta_s\right) = a_d\sin\left(\delta_d\right)$$

respectively.

7.3.2 Phase U-spin assumption

In this scenario it is assumed that $\delta_s = \delta_d$, but no assumption is made about the relative values of a_s and a_d. Equations 46 and 47 imply the following relation

$$\frac{\tan\phi_d+\gamma}{\tan\phi_s+\gamma} = \left[\frac{\tan\delta_d}{\tan\delta_s}\right]\left[\frac{\langle S_s\rangle_-}{\langle S_s\rangle_+}\right]\left[\frac{\langle S_d\rangle_+}{\langle S_d\rangle_-}\right], \tag{50}$$

which can then be used to extract γ unambiguously from the four CP-observables $\langle S_{s,d}\rangle_{+,-}$. The theoretical uncertainty in this extraction results from U-spin breaking corrections to $\delta_s = \delta_d$ only.

7.3.3 Amplitude U-spin assumption

In this scenario, it is assumed that $a_s = a_d$, but no assumption is made about the values of δ_s or δ_d. The exact relation

$$\left(\frac{a_s}{a_d}\right)R = \sigma\left|\frac{\sin(2\phi_d+2\gamma)}{\sin(2\phi_s+2\gamma)}\right|\sqrt{\frac{\langle S_s\rangle_+^2\cos(\phi_s+\gamma)^2+\langle S_s\rangle_-^2\sin(\phi_s+\gamma)^2}{\langle S_d\rangle_+^2\cos(\phi_d+\gamma)^2+\langle S_d\rangle_-^2\sin(\phi_d+\gamma)^2}}, \tag{51}$$

which follows from Equation 39 and the definitions of a_q and R given before, is used to extract γ. The parameter σ governs the sign of the right hand side, so that

$$\sigma = -sgn\left[\langle S_s\rangle_+\langle S_d\rangle_+\sin(\phi_d+\gamma)\sin(\phi_s+\gamma)\right], \tag{52}$$

if $\cos\delta_s$ and $\cos\delta_d$ are assumed to have the same sign, while

$$\sigma = -sgn\left[\langle S_s\rangle_-\langle S_d\rangle_-\cos(\phi_d+\gamma)\cos(\phi_s+\gamma)\right], \tag{53}$$

if $\sin\delta_s$ and $\sin\delta_d$ are assumed to have the same sign.

7.4 Fitting to the CP-observables

In the combined extraction, fitting to the CP-observables is done using the same toy Monte Carlo as in the previous section. The fitted parameters are $S_d, \overline{S}_d$, as defined in Equation 15 and 16, while the parameters $C_d, \overline{C}_d$ are fixed to be ± 1 in the fit, which is an excellent approximation. Because C_d is fixed, no knowledge of the parameter x_d is required, so that the fitted precisions on $S_d, \overline{S}_d$ only depend on the number of events and any systematic effects from the time resolution and imperfect knowledge of the mistag and background. As before, the mistag rate is left as a free parameter in the fit, thus eliminating that source of systematic error. For the channel $B_s^0 \to D_s^- K^+$ Equation 45 has been used to provide an additional constraint on the parameters $S_s, \overline{S}_s$, improving the precision with which they are extracted. Table 5 shows the precisions on the CP-observables, mistag, and x_s, which do not depend on the values of γ, ϕ_d or δ_d.

The CP-observables $S, \overline{S}$ are typically of order $S_d \sim O(0.01)$ and $S_s \sim O(0.1)$. $S_d, \overline{S}_d$ have been measured by B-factories in the B_d^0 sector, with a current world precision of ± 0.04 [ea06d]. This precision will improve by the time LHCb starts taking data, and B-factory data will be combined with data from LHCb to yield the best possible constraint on γ. At the time of writing, there has been no observation of CP violation in the decays $B_s^0 \to D_s^- K^+$.

7.5 Sensitivity to γ

Since the extraction of γ can proceed in any one of the three ways reviewed in Section 7.3, it will be necessary to perform a case study for each of these extraction scenarios. In particular, it is useful to concentrate on the sensitivity of these extraction scenarios to U-spin breaking effects, as well as their sensitivity to the input values of the parameters γ and $\delta_{s,d}$.

The inputs to the combined analysis are given in Table 6. Although the CP-observables will have associated systematic errors, the dominant systematic errors within the combined analysis

Table 5: A summary of the statistical precisions on the CP-observables $S_q, \overline{S}_q$, the mistag rate ω_q, and x_s in the channels $B_d^0 \to D^-\pi^+$ and $B_s^0 \to D_s^- K^+$ for one and five years of running, corresponding to 2 fb^{-1} and 10 fb^{-1} of data respectively.

	ω_d	S_d	$\overline{S}_d$	ω_s	S_s	$\overline{S}_s$	x_s
σ_{1y}	0.1%	0.0105	0.0105	0.3%	0.11	0.10	0.066
σ_{5y}	0.05%	0.0046	0.0046	0.13%	0.049	0.045	0.029

Table 6: Input parameter values to the combined analysis toy Monte Carlo.

Parameter	x_s	x_d	λ	ϕ_d	ϕ_s	R_b
Value	0.37	0.0175	0.22	47°	0°	17.2

are expected to come from U-spin breaking effects. Therefore, only the statistical errors on the CP-observables will be considered in this study. Also, it is assumed that ϕ_s, ϕ_d, and R_b are known exactly. In the case of R_b, this assumption is justified because the precisions on x_s from the channel $B_s^0 \to D_s^- K^+$ imply a relative error of $\sim 4\%$ on R_b after one year of data taking. This error is both negligible compared to the errors on the CP-observables, especially in the B_s sector, and it is also likely to be negligible compared to U-spin breaking effects. Effects such as time resolution, mistag, background, and the lifetime acceptance have been taken into account when determining the statistical errors on $S_q, \overline{S}_q$. Finally, since the channels in question are expected to be insensitive to new physics, the usual assumption that γ lies between 0° and 180° degrees will be used throughout.

In principle, it is possible to use all four Equations 46, 47, 50, and 51 in order to extract γ unambiguously. These four extractions are complementary, not only because they allow for the extraction of γ under different assumptions, but also because they afford varying precisions and discrimination between ambiguities depending on the values of γ and $\delta_{s,d}$. The contour plots shown in this section are to be read as follows

- The vertical axis describes the level of U-spin breaking, with 1 (thick horizontal line) corresponding to perfect U-spin symmetry for the quantities shown.
- The dashed straight lines enclose the region of $\pm 30\%$ U-spin breaking. Although there is no precise estimate of the likely level of U-spin breaking, 30% is a conservative assumption, since U-spin is expected to be a better symmetry than SU(3) in these decays. The expected level of SU(3) breaking was discussed in Section 3, and given as 10%.
- The thick curved line is the value of γ which would be measured given the appropriate level of U-spin symmetry breaking, assuming that the CP-observables $S_q, \overline{S}_q$ were perfectly known. It crosses the perfect U-spin symmetry line at the input value of γ, in this case 60°.
- The dashed curved lines are the 1σ contours, representing the uncertainty on the CP-observables $S_q, \overline{S}_q$.
- The triangle marks the location of the input value of γ.
- The upside down triangles mark the ambiguous solutions coming from the conventional $B_d^0 \to D^+\pi^-$ analysis.

Two particular scenarios, corresponding to large and small strong phase differences, will be considered in detail, followed by a more general overview of the performance.

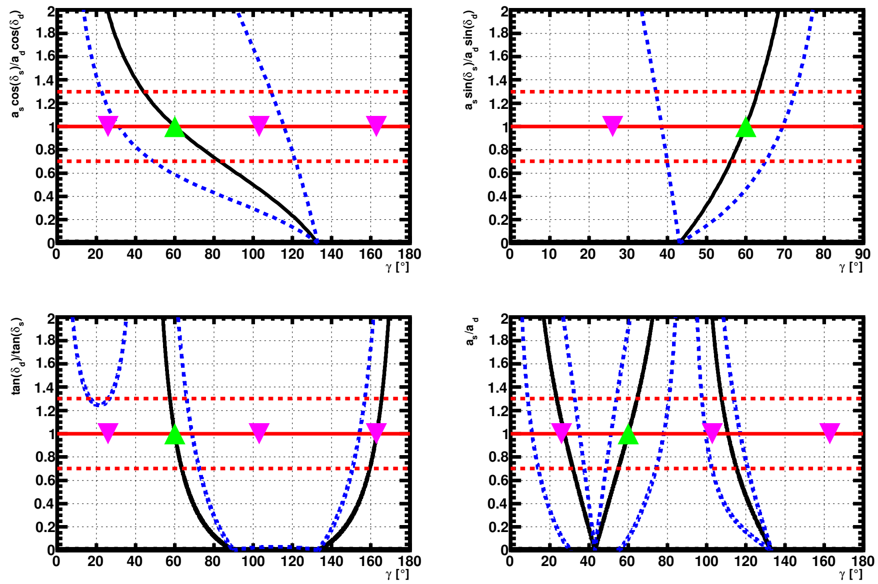

Figure 13: Contours in γ – U-spin breaking space for one year of data taking, with $\gamma = 60^\circ$ and $\delta_{s,d} = 60^\circ$. The four scenarios shown correspond, clockwise from top left, to Equations 46 (strong U-spin), 47 (strong U-spin), 51 (amplitude U-spin), and 50 (phase U-spin).

7.5.1 Error estimation

In the examples given, the errors are estimated from the intersection of the 1σ contours with horizontal lines indicating a $\pm 30\%$ level of U-spin symmetry breaking. In particular, consider Figure 14, and the contours for Equation 47. The 1σ contours and $\pm 30\%$ U-spin breaking lines define a region, whose upper right corner corresponds to the maximum positive error (systematic+statistical), while its lower left corner corresponds to the maximum negative error for the 1σ contours, assuming that U-spin breaking is limited to $\pm 30\%$. The negative error is taken from that contour for which the negative error is smallest (in this case Equation 47), while the positive error is independently taken from that contour for which the positive error is smallest. In this case the positive error is also smallest for Equation 47, but in principle the positive and negative errors could be obtained from different contours.

Such an error estimation procedure is not optimal, because it does not use all the available information. For one thing, the U-spin breaking is assumed to contribute a flat error, when in reality it should be estimated by a Gaussian of appropriate width. In addition, each of the four sets of contours is considered independently, when in reality they should be considered together. Instead of drawing 1σ bands for each U-spin assumption, the correct procedure would be to calculate the PDF in γ–(U-spin breaking) space using all four assumptions and accounting for the correlations between them. Take as an example the contours associated with Equations 46 and 47: these are produced from orthogonal combinations of independent (ignoring correlations) variables, and are themselves independent. Therefore they could be multiplied together to produce a joint PDF in γ–(U-spin breaking) space. The 1σ contours in γ would then be calculated by projecting the resulting PDF onto the γ axis. The current procedure is akin to projecting the PDF associated with each assumption before combining them.

7.5.2 $\gamma = 60^\circ$ and $\delta_{s,d} = 60^\circ$

The contour plots for this scenario are shown in Figure 13 for one year of data taking, and in Figure 14 for five years of data taking. After one year of data taking, the strong U-spin assumption of Equation 47 already disfavours all ambiguous solutions, even allowing for a 30% U-spin breaking

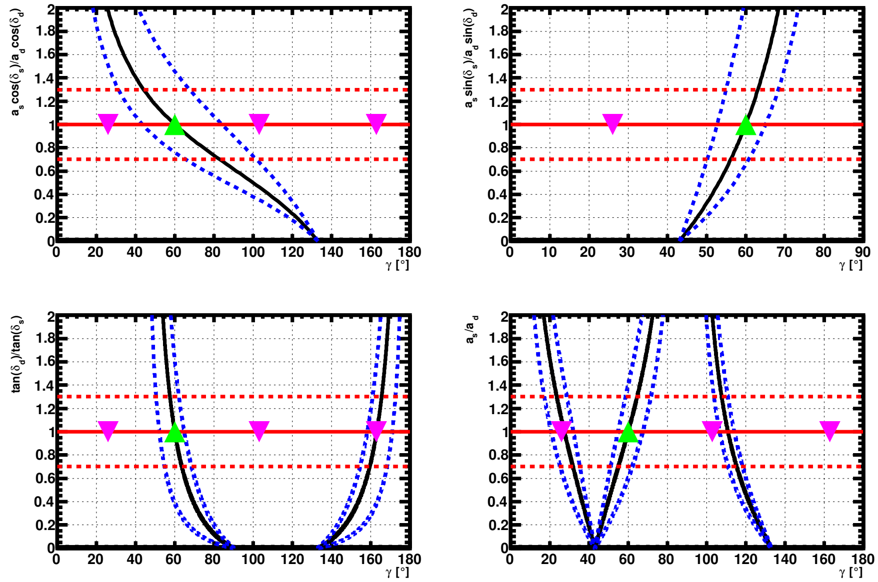

Figure 14: Contours in γ – U-spin breaking space for five years of data taking, with $\gamma = 60^\circ$ and $\delta_{s,d} = 60^\circ$. The four scenarios shown correspond, clockwise from top left, to Equations 46 (strong U-spin), 47 (strong U-spin), 51 (amplitude U-spin), and 50 (phase U-spin).

correction. The statistical precision is -21°,$+9^\circ$, while a 30% U-spin breaking correction introduces an additional $\pm 3^\circ$ systematic error. The phase U-spin assumption provides an upper statistical error on γ of 10°. Although the ambiguous solution at $\sim 160^\circ$ is not disfavoured by this assumption, it is disfavoured for most scenarios by the other three relations. The amplitude U-spin assumption provides a statistical precision of -8°,$+14^\circ$, and a 30% U-spin breaking correction introduces an additional $\pm 4^\circ$ systematic error. Once again, ambiguous solutions are disfavoured when all four relations are considered together.

After five years, the strong U-spin assumption of Equation 47 gives a statistical precision of -8°,$+5^\circ$, while a 30% U-spin breaking correction introduces an additional $\pm 2^\circ$ systematic error. All ambiguous solutions are now heavily disfavoured for any U-spin breaking correction for which $a_s \sin(\delta_s)$ has the same sign as $a_d \sin(\delta_d)$. The phase U-spin assumption now also gives a statistical precision of $-7^\circ, +5^\circ$, while a 30% U-spin breaking correction introduces an additional -2°,$+3^\circ$ systematic error. The amplitude U-spin assumption affords a statistical precision of $-5^\circ, +7^\circ$, while a 30% U-spin breaking correction introduces a systematic of $\pm 3^\circ$. When all four relations are considered together, it is clear that all ambiguous solutions are excluded after five years of data taking.

7.5.3 $\gamma = 60^\circ$ and $\delta_{s,d} = 10^\circ$

Now consider the same value of γ, but much smaller strong phases. The contour plots are shown in Figure 15 for one year of data taking, and in Figure 16 for five years of data taking. After one year, none of the four relations provide effective discrimination against ambiguities. The best resolution comes from using the strong U-spin assumption of Equation 46, which reduces the ambiguity on γ to a twofold one, and gives a statistical precision of -20°,$+30^\circ$. After five years, the strong U-spin assumption of Equation 46 gives a statistical precision of -8°,$+10^\circ$, while the phase U-spin assumption gives an upper statistical precision of $+12^\circ$, however it is much less sensitive to U-spin breaking effects, with an upper systematic error of $+4^\circ$ associated with a 30% level of U-spin breaking. Equation 46 is now beginning to disfavour the solution at $\sim 53^\circ$ under exact U-spin symmetry. In general, Equation 46 is the only relation which provides any discrimination when the strong phases are small, and this area of parameter space is where the combined extraction

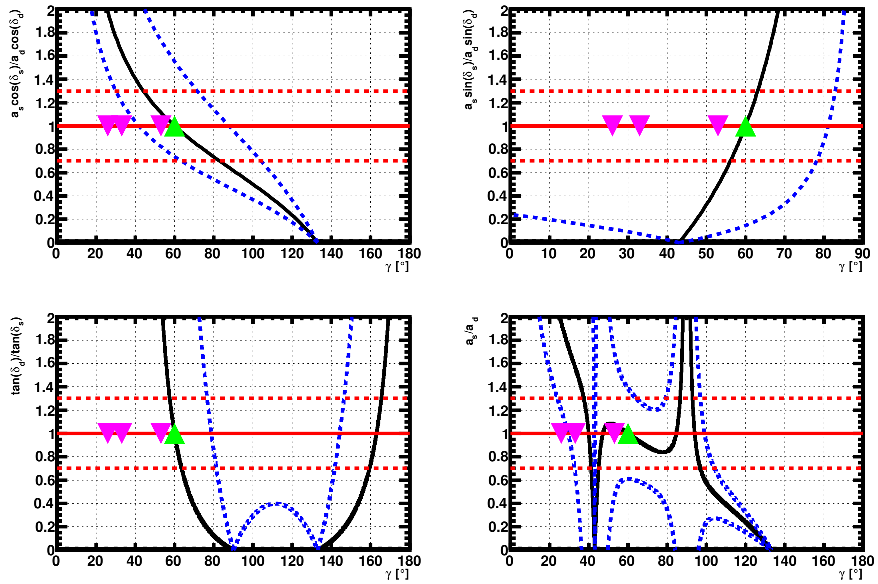

Figure 15: Contours in γ – U-spin breaking space for one year of data taking, with $\gamma = 60^\circ$ and $\delta_{s,d} = 10^\circ$. The four scenarios shown correspond, clockwise from top left, to Equations 46 (strong U-spin), 47 (strong U-spin), 51 (amplitude U-spin), and 50 (phase U-spin).

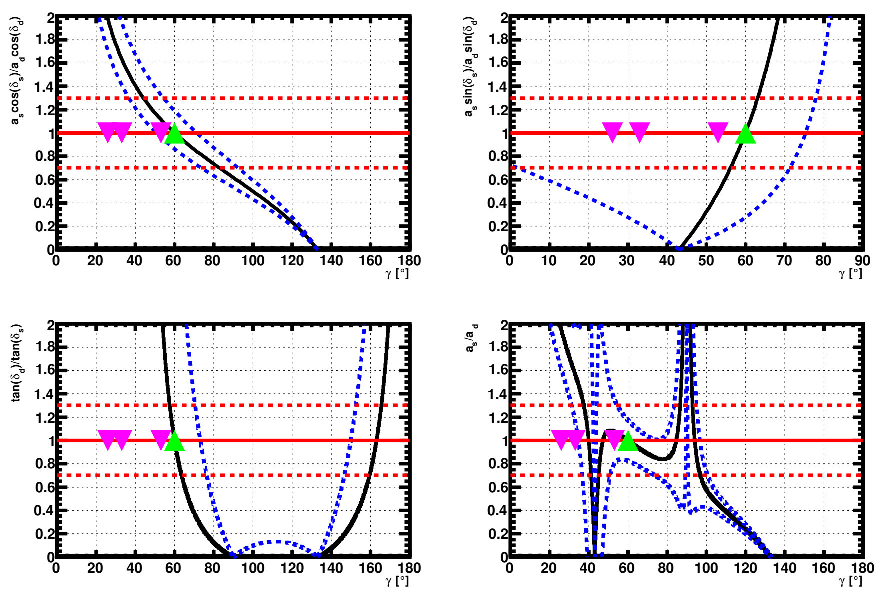

Figure 16: Contours in γ – U-spin breaking space for five years of data taking, with $\gamma = 60^\circ$ and $\delta_{s,d} = 10^\circ$. The four scenarios shown correspond, clockwise from top left, to Equations 46 (strong U-spin), 47 (strong U-spin), 51 (amplitude U-spin), and 50 (phase U-spin).

performs least well.

7.6 Performance summary

The specific values of γ and the strong phases affect the combined extraction in two important ways. Firstly, certain combinations of $\gamma, \delta_s, \delta_d$ can lead to ambiguous γ solutions separated by only a few degrees, which will be impossible to distinguish even after many years of running. Secondly, the width of the error contours in U-spin/γ space varies with the values of $\gamma, \delta_s, \delta_d$. Consider Equation 47, modified to take into account the errors on $\langle S_{s,d}\rangle_-$:

$$\left[\frac{a_s \sin\delta_s}{a_d \sin\delta_d}\right] R = -\left(-1\right)^{L_s - L_d}\left[\frac{\cos\left(\phi_d+\gamma\right)}{\cos\left(\phi_s+\gamma\right)}\right]\left[\frac{\langle S_s\rangle_- \pm \sigma_{\langle S_s\rangle_-}}{\langle S_d\rangle_- \pm \sigma_{\langle S_d\rangle_-}}\right]. \tag{54}$$

If the error on $\langle S_{s,d}\rangle_-$, $\sigma_{\langle S_{s,d}\rangle_-}$, is greater than the value of $\langle S_{s,d}\rangle_-$ itself, the sign of this observable will be badly defined, and the corresponding error contour will not provide a useful constraint on γ. An example of this effect was seen in the scenario with small strong phases above, where it is precisely this effect that prevents Equation 47 from usefully constraining γ, even after five years of running.

This uncertainty on the sign of $\langle S_{s,d}\rangle_\pm$ also causes the achievable precision on γ to be limited by the errors on $\langle S_d\rangle_\pm$, not $\langle S_s\rangle_\pm$. Although the errors on $\langle S_d\rangle_\pm$ are much smaller than those on $\langle S_s\rangle_\pm$, the fact that $x_s \gg x_d$ means that $\left|\langle S_s\rangle_\pm\right| \gg \left|\langle S_d\rangle_\pm\right|$, and the parameters $\langle S_d\rangle_\pm$ are therefore more susceptible to being measured with an incorrect sign. For example, when $\gamma = 60°$ and $\delta_{s,d} = 60°$, the CP-observables are

$$\begin{aligned}\langle S_d\rangle_- &= -0.012,\\ \langle S_d\rangle_+ &= 0.023,\\ \langle S_s\rangle_- &= 0.28,\\ \langle S_s\rangle_+ &= -0.28,\end{aligned}$$

while the errors are given by

$$\begin{aligned}\sigma_{\langle S_d\rangle_\pm} &= 0.0105,\\ \sigma_{\langle S_s\rangle_\pm} &= 0.011.\end{aligned}$$

Notice the doubling of the error on $\langle S_s\rangle_\pm$ will not change the sign of $\langle S_s\rangle_\pm$, but doubling the error on $\sigma_{\langle S_d\rangle_\pm}$ will change the sign of $\langle S_d\rangle_-$, rendering Equation 47 of limited use in constraining γ. It is important not to allow the small errors on $\langle S_d\rangle_\pm$ to obscure the fact that it is these parameters that need to be known most precisely for the combined analysis to fulfil its potential.

Table 7 presents the errors for the two scenarios shown above. The upper error quoted in any one γ, δ scenario is the smallest upper error in any one of the four U-spin assumptions, and similarly for the lower error. For example, it is possible for the quoted upper error in a scenario to come from the strong U-spin assumption, while the lower error comes from the phase U-spin assumption. The statistical and systematic error are always quoted from the same U-spin assumption.

It turns out that $\gamma = 60°$ is particularly favourable for this extraction, because none of the four CP-observables $\langle S_{s,d}\rangle_\pm$ is then particularly small. Looking back at Equation 39, the $\sin\left(\phi_q+\gamma\right), \cos\left(\phi_q+\gamma\right)$ terms control the size of $\langle S_{s,d}\rangle_\pm$. For $\gamma = 60°$, $\phi_d+\gamma = 107°$ and $\phi_s+\gamma = 60°$, so that all four sine and cosine terms are substantial, but for values of γ significantly higher or lower than $60°$ these terms may approach 0, limiting precision regardless of the values of the strong phases. Finally, the performance for negative strong phases will be exactly the same as for positive strong phases of the same magnitude, as long as δ_s and δ_d have the same sign.

7.7 Summary of combined extraction

The combined U-spin analysis of the channels $B_d^0 \to D^-\pi^+$ and $B_s^0 \to D_s^- K^+$ allows for an unambiguous extraction of γ under a variety of theoretical assumptions. It also has a great advantage

Table 7: One and five year precisions on γ for the scenarios considered in this note, giving the statistical error and the systematic error associated with a 30% U-spin breaking.

	$\sigma_{1y}^{\text{stat}}$	$\sigma_{1y}^{\text{syst}}$	$\sigma_{5y}^{\text{stat}}$	$\sigma_{5y}^{\text{syst}}$
$\gamma = 60°$,$\delta_{s,d} = 60°$	$-9°, +9°$	$-4°, +3°$	$-5°, +5°$	$\pm 3°$
$\gamma = 60°$,$\delta_{s,d} = 10°$	$-20°, +30°$	$-10°, +22°$	$-8°, +12°$	$-15°, +4°$

over the "conventional" extraction of not requiring $\langle x_d \rangle$ to be resolved, since $\langle x_d \rangle$ only enters the expressions for γ as a second order correction through the term $1 + \langle x_q \rangle^2$, which is negligible.

Even if this combined analysis is outperformed by other analyses at measuring γ, it can instead be used to learn about the scale of U-spin symmetry breaking. For example, under perfect U-spin symmetry, the untagged rate analysis and the U-spin analysis can be expected to return the same value of γ, since the experimental systematics will be broadly similar in the B_s and B_d systems[4)]. Any observable difference between the fitted values of γ can therefore be used to constrain the U-spin breaking parameters. Finally, the U-spin analysis may allow a limit to be set on a_s/a_d in conjunction with other tree level measurements of γ. It may then be possible to use the expression

$$\frac{a_s}{a_d} = \left(\frac{\lambda^2}{1 - \lambda^2} \right) \left| \frac{x_s}{x_d} \right|, \tag{55}$$

to make an indirect measurement of x_d, since x_s will be large enough to measure from the asymmetries in $B_s^0 \to D_s^- K^+$ alone.

8 Conclusion

The CKM angle γ can be extracted from the decay mode $B_d^0 \to D^- \pi^+$ with a precision which depends significantly on the values of the parameters δ_d and $\phi_d - \gamma$, as well as the assumed error on the knowledge of x_d. The value of the mistag in this channel can be fitted from the asymmetries independently of any external information about its value, which eliminates one significant source of systematic error in the fit. The achievable precision on γ depends on the lifetime distribution of the selected B_d^0 mesons, with samples richer in longer lived B_d^0 particles affording a better sensitivity to γ. The precision achievable on the value of γ depends significantly on the knowledge of the parameter x_d, which must be established from external sources.

Because of these difficulties, a combined analysis of the channels $B_d^0 \to D^- \pi^+$ and $B_s^0 \to D_s^- K^+$ has been pursued. The method's viability has been demonstrated through a toy Monte Carlo incorporating significant amounts of realism, including background, mistag, proper time resolution, and the proper time acceptance. The precision on γ, and the viability of excluding ambiguous solutions, is found to have a significant dependence on the precise input values of γ and the strong phases $\delta_{d,s}$. With the preferred Standard Model value $\gamma = 60°$ and large strong phases, it is possible to achieve a statistical precision of $<5°$ after five years of data taking, while excluding all ambiguous solutions. Other scenarios, such as small strong phases, or low values of γ, make an unambiguous extraction more difficult, and reduce the statistical precision achievable after five years of data taking to $\sim 10°$, with a systematic error of $\sim 15°$.

Finally, these methods can be applied directly to the decay modes $B_s^0 \to D_s^- K^{*+}$, $B_d^0 \to D^- \rho^+$, $B_s^0 \to D_s^{*-} K^+$, $B_d^0 \to D^{*-} \pi^+$, and work is ongoing on a combined extraction of γ from all of these modes. A brief discussion of the possible improvement achievable by including the decay mode $B_d^0 \to D^{*-} \pi^+$ is included in Appendix A.

[4)] In particular, the mistag rate can be fitted from the asymmetries in both $B_d^0 \to D^- \pi^+$ and $B_s^0 \to D_s^- K^+$, the proper time resolutions are expected to be similar, as are the lifetime acceptance functions.

Acknowledgements

The authors of this note would like to acknowledge Jonas Rademacker, whose previous work on measuring γ using the decay mode $B_d^0 \rightarrow D^{*-}\pi^+$ at LHCb was the basis for this study. The authors would also like to acknowledge helpful discussions with Jim Libby, in particular with regards to generating and fitting toy Monte Carlo events.

A Including information from $B_d^0 \to D^{*\pm}\pi^{\mp}$

The decay mode $B_d^0 \to D^{*\pm}\left(D^0\pi^{\pm}\right)\pi^{\mp}$ depends on γ in an analogous way to $B_d^0 \to D^{\pm}\pi^{\mp}$, and therefore naturally complements the study presented in this note. Indeed the extraction of γ from this mode has already been studied at LHCb [Rad01]. The most recent selection study [AE03] found LHCb could expect to reconstruct 206,000 $B_d^0 \to D^{*\pm}\left(D^0\pi^{\pm}\right)\pi^{\mp}$ fully triggered decays in 2 fb^{-1} of data taking with an exclusive reconstruction technique. Additionally, an inclusive reconstruction technique, where the D^0 is assumed to decay into two charged particles plus anything else, and the momenta of the two pions are used to reconstruct the B momentum, has been shown [Rad01] to yield 867,000 fully triggered signal events in 2 fb^{-1} of data taking. It is interesting to explore the contribution this decay mode can make to the extraction of γ from $B_d^0 \to D^{\pm}\pi^{\mp}$.

From an experimental point of view, the inclusive reconstruction of $B_d^0 \to D^{*\pm}\left(D^0\pi^{\pm}\right)\pi^{\mp}$ leads to a proper time resolution of 170 fs, approximately four times worse than in $B_d^0 \to D^{\pm}\pi^{\mp}$. In addition, the mass resolution is considerably worse. On the other hand, the mass difference between the $D^{*\pm}$ and D^0 remains a powerful background discriminant even in the inclusive reconstruction, while the $D^{*\pm}$ decay mode may benefit from a higher interference [ea08] between its tree level diagrams, and hence a higher intrinsic sensitivity to γ. The $D^{*\pm}$ and $D^{\pm}$ modes can be expected to have the same flavour tagging performance. For the purposes of this appendix, the precisions on the CP-observables in $B_d^0 \to D^{*\pm}\left(D^0\pi^{\pm}\right)\pi^{\mp}$ are assumed equal to the precisions in $B_d^0 \to D^{\pm}\pi^{\mp}$, **for an equal number of events**. Assuming the inclusive reconstruction technique is used, and scaling the precisions in Table 5 for the smaller annual yield of the $D^{*\pm}$, the precision on the CP observables after 2 fb^{-1} of data taking is found to be $\sigma_{S_{d^*}} = 0.0134$.

From a theoretical point of view, the mode $B_d^0 \to D^{*\pm}\left(D^0\pi^{\pm}\right)\pi^{\mp}$ has the additional interest that its strong phase is expected [Fle03] to be 180° away from the strong phase of $B_d^0 \to D^{\pm}\pi^{\mp}$: $\delta_{d^*} = \delta_d - 180°$. This allows the combined γ precision from $B_d^0 \to D^{*\pm}\left(D^0\pi^{\pm}\right)\pi^{\mp}$ and $B_d^0 \to D^{\pm}\pi^{\mp}$ to be better than a naive addition in quadrature, because the discrimination between ambiguous solutions is improved as well as the statistical precision on each solution. For a clear example of this, consider the precision achievable after 10 fb^{-1} of data taking in the case where $\gamma = 60°$ and $\delta_d = 60°$. Figure 8 shows the precision from $B_d^0 \to D^{\pm}\pi^{\mp}$ alone, where the ambiguous solutions are not resolved at the 1 σ level. The result of including the $B_d^0 \to D^{*\pm}\left(D^0\pi^{\pm}\right)\pi^{\mp}$ data, and assuming that $\delta_{d^*} = \delta_d - 180°$ is shown in Figure 17. All ambiguous solutions are now more than 1 σ away from each other, and the measured value of γ at the "correct" solution is

$$\gamma_{5\text{y}} = \left(61^{-8}_{+10}\right)^{\circ}.$$

Note that this has been achieved without any U-spin assumptions about the size of the strong phases, and making such assumptions will further improve the achievable precision, as well as excluding ambiguous solutions. Studying the strong phases in the U-spin related decay channels $B_s^0 \to D_s^{\pm}K^{\mp}$ and $B_s^0 \to D_s^{*\pm}K^{\mp}$ will also provide an interesting cross check of the assumption that $\delta_{d^*} = \delta_d - 180°$.

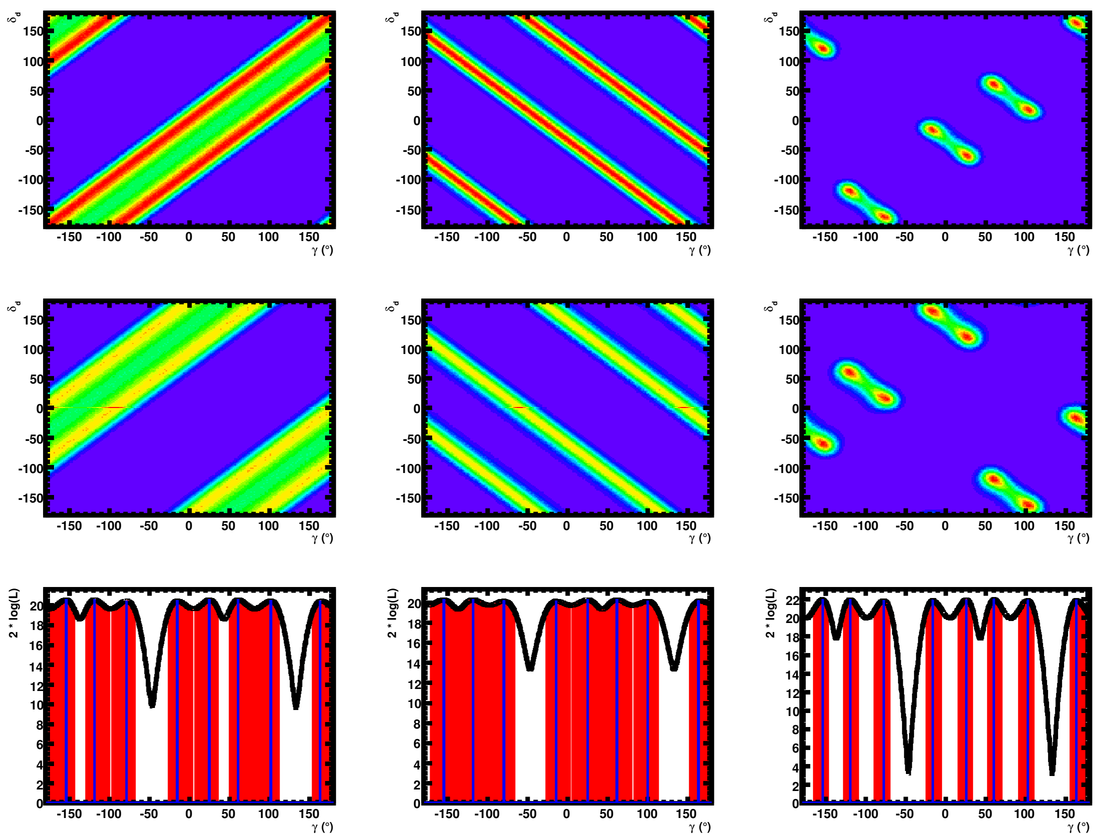

Figure 17: Contour plots showing the constraints in the δ_{d,d^*} - γ plane. Top row: from S_d (top left), $\overline{S}_d$ (top middle), and the combined constraint from S_d and $\overline{S}_d$ (top right). Middle row: from S_{d^*} (middle left), $\overline{S}_{d^*}$ (middle middle), and the combined constraint from S_{d^*} and $\overline{S}_{d^*}$ (middle right). Bottom row: projected combined constraint from S_d and $\overline{S}_d$ (bottom left), projected combined constraint from S_{d^*} and $\overline{S}_{d^*}$ (bottom middle), projected total constraint from all four observables (bottom right). The likelihood projection in γ is shown in the bottom three plots. Warmer colours indicate a greater probability density. The blue line(s) correspond to the central value(s) for γ, while the red area indicates the 1σ interval corresponding to the central value(s). This plot is made with input values of $\gamma = 60^\circ$, $\delta_d = 60^\circ$, $\delta_{d^*} = -120^\circ$, five years of data taking, and a 10% uncertainy on the assumed values of x_d, x_{d^*}. A constraint of $\delta_{d^*} = \delta_d - 180^\circ$ is applied when calculating the likelihood. Note that the units of δ_d on the vertical axes are degrees.

References

[AE03] L. Allebone and U. Egede. Exclusive selection of $B_d^0 \to D^{*-}\pi^+$. Technical Report CERN-LHCb-2003-126, CERN, Geneva, 2003.

[All06] J. et al. Allison. Geant4 developments and applications. *IEEE Trans. Nucl. Sci.*, 53:270, 2006.

[Baa07] M. Baak. Ph.D. thesis report, 2007. SLAC-R-858.

[BNSVH07] J. Borel, L. Nicolas, O. Schneider, and J. Van Hunen. The $B_s^0 \to D_s^{\mp}\pi^{\pm}$ and $B_s^0 \to D_s^{\mp}K^{\pm}$ selections. Technical Report CERN-LHCb-2007-017, CERN, Geneva, 2007.

[BR97] R. Brun and F. Rademakers. ROOT: An object oriented data analysis framework. *Nucl. Instrum. Meth.*, A389:81, 1997.

[CLM07] M. Calvi, O. Leroy, and M. Musy. Flavour tagging algorithms and performances in LHCb. Technical Report CERN-LHCb-2007-058, CERN, Geneva, May 2007.

[CMR07] S. Cohen, M. Merk, and E. Rodrigues. $\gamma + \phi_s$ sensitivity studies from combined $B_s^0 \to D_s^{\mp}\pi^{\pm}$ and $B_s^0 \to D_s^{\mp}K^{\pm}$ samples at LHCb. Technical Report CERN-LHCb-2007-041, CERN, Geneva, 2007.

[ea05a] The CDF Collaboration (D. E. Acosta et al.). Measurement of the lifetime difference between B_s^0 mass eigenstates. *Phys. Rev. Lett.*, 94:101803, 2005.

[ea05b] The CKMfitter Group (J. Charles et al.). updated results and plots available at: http://ckmfitter.in2p3.fr. *Eur. Phys. J.*, C41:1, 2005.

[ea06a] Heavy Flavor Averaging Group (E. Barberio et al.). Averages of b-hadron properties at the end of 2006, 2006. hep-ex/0704.3575v1.

[ea06b] The BaBar Collaboration (B. Aubert et al.). Measurement of time-dependent CP asymmetries in $B^0 \to D^{(*)\pm}\pi^{\mp}$ and $B^0 \to D^{\pm}\rho^{\mp}$ decays. *Phys. Rev.*, D73:111101, 2006.

[ea06c] The Belle Collaboration (F. J. Ronga et al.). Measurements of CP violation in $B^0 \to D^{*-}\pi^+$ and $B^0 \to D^-\pi^+$ decays. *Phys. Rev.*, D73:092003, 2006.

[ea06d] W.-M.Yao et al. Particle Data Group. *J. Phys.*, G33(1), 2006.

[ea07] The D0 Collaboration (V. M. Abazov et al.). Lifetime difference and CP-violating phase in the B_s^0 system. *Phys. Rev. Lett.*, 98:121801, 2007.

[ea08] The BaBar Collaboration (B. Aubert et al.). Measurement of the Branching Fractions of the Rare Decays $B^0 \to D_s^{(*)+}\pi^-$, $B^0 \to D_s^{(*)+}\rho^-$, and $B^0 \to D_s^{(*)-}K^{(*)+}$, 2008. hep-ex/0803.4296.

[Fle03] R. Fleischer. New strategies to obtain insights into CP violation through $B_s \to D_s^{\pm}K^{\mp}, D_s^{*\pm}K^{\mp}, ...$ and $B_d \to D^{\pm}\pi^{\mp}, D^{*\pm}\pi^{\mp}, ...$ decays. *Nucl. Phys.*, B657:459, 2003.

[Gli07] V. Gligorov. Reconstruction of the Channel $B_d^0 \to D^+\pi^-$ and Background Classification at LHCb. Technical Report CERN-LHCb-2007-044, CERN, 2007.

[JR75] F. James and M. Roos. Minuit: A System for Function Minimization and Analysis of the Parameter Errors and Correlations. *Comput. Phys. Commun.*, 10:343, 1975.

[Rad01] J. Rademacker. Evaluation of the LHCb RICH detectors and a measurement of the CKM angle γ, 2001. CERN-THESIS-2001-017.

[SMS06] Torbjorn Sjostrand, Stephen Mrenna, and Peter Skands. PYTHIA 6.4 physics and manual. *JHEP*, 05:026, 2006.

[SS07] A. Soni and D. Suprun. Determination of γ from charmless $B \to M^{(1)}M^{(2)}$ decays using U-spin. *Phys. Rev.*, D75:054006, 2007.

[Wil05] G. Wilkinson. Extraction of γ at LHCb with a Combined $B_s \to D_s^{\pm}K^{\mp}$ and $B_d \to D^{\pm}\pi^{\mp}$ Analysis. Technical Report CERN-LHCb-2005-036, CERN, Geneva, 2005.